Electron-impact excitation of molecular hydrogen

Mark C. Zammit, Jeremy S. Savage, Dmitry V. Fursa, and Igor Bray

Phys. Rev. A **95**, 022708 — Published 6 February 2017

DOI: 10.1103/PhysRevA.95.022708

Electron impact excitation of molecular hydrogen

Mark C. Zammit[1,2],* Jeremy S. Savage[2], Dmitry V. Fursa[2], and Igor Bray[2]
[1] *Theoretical Division, Los Alamos National Laboratory, Los Alamos, New Mexico 87545, USA and*
[2] *Curtin Institute for Computation and Department of Physics, Astronomy and Medical Radiation Sciences, Curtin University, Perth, Western Australia 6102, Australia*
(Dated: January 11, 2017)

We report the electron impact integrated and differential cross sections for excitation to the $b\ ^3\Sigma_u^+$, $a\ ^3\Sigma_g^+$, $c\ ^3\Pi_u$, $B\ ^1\Sigma_u^+$, $E, F\ ^1\Sigma_g^+$, $C\ ^1\Pi_u$, $e\ ^3\Sigma_u^+$, $h\ ^3\Sigma_g^+$, $d\ ^3\Pi_u$, $B'\ ^1\Sigma_u^+$, $D\ ^1\Pi_u$, $B''\ ^1\Sigma_u^+$, $D'\ ^1\Pi_u$ states of molecular hydrogen in the energy range from 10 to 300 eV. Total scattering and total ionization cross sections are also presented. The calculations have been performed using the convergent close-coupling method within the fixed-nuclei approximation. Detailed convergence studies have been performed with respect to the size of the close-coupling expansion and a set of recommended cross sections has been produced. Significant differences with previous calculations are found. Agreement with the experiment is mixed, ranging from excellent to poor depending on the transition and incident energy.

PACS numbers: 34.50.Gs,52.20.Fs

I. INTRODUCTION

Accurate electron-impact electronic excitation cross sections of molecular hydrogen are important for modeling various plasmas. The applications range from plasma processing to astrophysics and fusion. A number of compilations of e-H_2 cross sections have been published [1–4] with the latest in 2008. For the grand total and ionization cross sections there are a substantial number of measurements from different research groups that are broadly in good agreement [5–12]. However the situation is very different for the electronic excitation cross sections where large discrepancies between various sets of measurements are common.

The most detailed experimental results come from the measurements of differential cross sections (DCS) [13–20] for which absolute normalization is a particularly difficult task. For angle integrated cross sections (ICS) additional errors arise from an extrapolation procedure utilized by experiment to obtain DCS at angles inaccessible by the experiment. There are a large number of optical excitation function measurements [21–27]. Such measurements provide relative cross sections that are affected by largely unknown cascades. Another difficulty in establishing accurate experimental cross sections is due to the complicated energy loss spectrum of the H_2 molecule. Different electronic-vibrational manifolds of H_2 overlap which requires sophisticated unfolding procedures and significantly affects the uncertainties of the experimental results. Despite these difficulties the most recent recommended cross sections [1] rely entirely on experiment.

Electron collisions with molecules is an inherently multi-centre problem. In addition to electronic excitation, reaction channels leading to molecular rotations, vibrations, and dissociation, as well as the lack of spherical symmetry, present special challenges. Within the Born-Oppenheimer approximation the electronic excitations can be effectively separated from the molecular rotations and vibrations. The fixed-nuclei (FN) approximation is a convenient way to further reduce the problem to electronic degrees of freedom only. With these approximations the electronic excitation processes in electron-molecule collisions are conceptually similar to those in electron-atom collisions and the experience gained in the latter is directly applicable to the former. Such experience tells us that the close-coupling method is the technique of choice to obtain reliable and accurate collision data. The close-coupling expansion must be sufficiently large and capable to model all important reaction channels including ionization processes. This is particularly important for the intermediate collision energies starting from the opening of ionization channels ($\sim$ 16 eV) to a few multiples of this threshold. Infinite number of bound states and the continuum of a target atom or molecule require the introduction of the techniques to represent them via a finite size (near complete) expansion. The *ab-initio* convergent close-coupling (CCC) method [28] and R-matrix with pseudostates (RMPS) method [29] are examples of such an approach in the case of electron-atom scattering.

Another important point is the quality of the target states used in the close-coupling expansion. The accuracy of target state energies, oscillator strengths for transition between bound states, and static dipole polarizability of the ground state to a large degree predetermine the accuracy of the collision calculations. While atomic and molecular structure can be obtained to high accuracy often a simpler model has to be adopted to make collision calculations feasible. This is particularly the case for electron-molecule collisions where multi-centre representation of the target wave functions poses an additional challenge. Expansions that utilize Gaussian functions are a common approach to address this problem. However, for large expansions the linear dependency of the basis

*electronic address: mzammit@lanl.gov

functions can become a problem and Gaussian functions are generally ill suited for the description of the continuum wave functions, particularly of the projectile electron.

The hydrogen molecule, for which wave functions are known to high accuracy, offers an attractive testing ground for the development of theoretical techniques in electron-molecule scattering. There have been many calculations of e-H_2 scattering. Earlier close-coupling calculations have been performed using a number of theoretical methods, such as the complex Kohn [30, 31] and Schwinger multichannel [32–34] variational methods, the linear algebraic [35] and continued fraction methods [35, 36]. They used simple single-configuration wave functions and included just two states (initial and final) in the close-coupling expansion except for Refs. [31, 36], where a four state expansion was used. There have been also a number of distorted-wave (DW) methods applied to e-H_2 scattering [37–39]. The most detailed results are due to the R-matrix (RM) calculations of Branchett et al. [40, 41] and the Schwinger multichannel (SMC) calculations of da Costa et al. [42] which both included the seven lowest non-degenerate states in the close-coupling expansion. The RM calculations have been performed for incident electron energies up to 20 eV and used an accurate configuration-interaction (CI) representation of the target wave functions. The SMC calculations have been conducted up to 30 eV but used less sophisticated CI wave functions compared to the RM method. The RMPS method was applied to e-H_2 scattering by Gorfinkiel and Tennyson [43] with the aim to obtain low energy ionization cross sections. The RMPS calculations had a maximum of 41 states in the close-coupling expansion but only the ground and first excited states were represented accurately. The time-dependent close-coupling (TDCC) method has also been used to calculate e-H_2 ionization [44] within a one-electron model.

It is not surprising that the agreement between theoretical results is poor as the sizes of the close-coupling expansions have been very small and the results are likely to be not convergent with the number of states used. In fact, no comprehensive convergence studies have ever been performed for e-H_2 cross sections. With a few exceptions the same applies to electron-molecule scattering in general. The aim of this paper is to present e-H_2 excitation cross sections obtained from large-scale close-coupling calculations performed using the molecular implementation of the CCC method. In this method a single-centre approach to molecular structure is adopted and a Sturmian (Laguerre) single-particle basis is used to represent molecular wave functions. The CCC method has been successfully applied to positron scattering from H_2 [45–47] and electron scattering from H_2^+ and its isotopologues [48, 49]. In both cases the use of a large Laguerre basis allowed us to demonstrate convergence of the calculated cross sections within the FN approximation and perform adiabatic-nuclei (AN) calculations for scattering from the hot (vibrationally) excited states.

In the preceding Letter [50] we have presented results for the elastic, total and ionization cross sections and DCS at 17.5 eV for selected excited states. Here we present detailed comparisons with the available experiments, perform detailed convergence studies for the DCS and ICS, and present a set of convergent excitation cross sections for e-H_2 scattering. The paper is organized as follows. In section II we outline the theoretical method and present details of the calculations. In section III we present the convergence studies and compare with previous calculations and experiments for the total cross section (TCS), total ionization cross section (TICS) and $b\ ^3\Sigma_u^+$, $a\ ^3\Sigma_g^+$, $c\ ^3\Pi_u$, $B\ ^1\Sigma_u^+$, $E,F\ ^1\Sigma_g^+$, $C\ ^1\Pi_u$, $e\ ^3\Sigma_u^+$, $h\ ^3\Sigma_g^+$, $d\ ^3\Pi_u$, $B'\ ^1\Sigma_u^+$, $D\ ^1\Pi_u$, $B''\ ^1\Sigma_u^+$, $D'\ ^1\Pi_u$ excitation cross sections. Conclusions and future directions for our work are presented in section IV. We use atomic units throughout unless otherwise specified.

II. MOLECULAR CCC METHOD

Application of the CCC method to electron-atom collisions has been reviewed extensively in Refs. [28, 51, 52] and its application to electron collisions with molecules has been recently detailed as well [48]. Here we give a brief overview of the method and present details specific for e-H_2 collisions. The nonrelativistic formulation of the CCC method is adopted in this work. The fully relativistic (Dirac equation) approach can be developed in the same way as it was done for electron-atom scattering [53, 54].

A. Theoretical method

The CCC method is formulated in the FN approximation [55]. Throughout the collision the nuclei are kept at a fixed orientation and internuclei distance R that is normally taken to be equal to the equilibrium distance of H_2, $R_0 = 1.40$, but other choices can be useful. In particular, the average internuclear distance of the ground vibrational level, $R_m = 1.448$, is arguably a better approximation (more details later in this section). Due to the separation of the electronic degrees of freedom from nuclei motion the problem is reduced to the solution of the electronic wave functions only. It is worthwhile to remember that information on nuclei motion can be recovered from the FN collision results by adopting the AN approximation [55] that requires the FN calculations to be performed at a number of internuclear distances. In what follows we will omit the explicit dependence on R.

The total electronic wave function of the e-H_2 collision system is expanded in the set of N target states of H_2

$$\Psi_i^{N(+)}(x_0,x_1,x_2) = \mathcal{A}\psi_i^{N(+)}(x_0,x_1,x_2) = \mathcal{A}\sum_{n=1}^{N} f_n^{N(+)}(x_0)\Phi_n^N(x_1,x_2), \quad (1)$$

where x is used to denote both the spatial and spin coordinates, the 0 index is used to denote the projectile space, the 1 and 2 indices are used for the target space, and (+) denotes outgoing spherical boundary conditions. The antisymmetrization operator is $\mathcal{A} = 1 - P_{01} - P_{02}$ and P_{0i} is the space exchange operator.

It is convenient to formulate the scattering equations in the body frame with the z-axis aligned along the internuclear line and the origin at the midpoint between the two nuclei of H_2. The total wave function is a solution of the Schrödinger equation

$$(E^{(+)} - H)\Psi_i^{N(+)} = 0, \tag{2}$$

where H is the total (electronic) Hamiltonian of the Schrödinger equation

$$H = H_0 + H_T + \sum_{i=1}^{2} V_{0i}. \tag{3}$$

Here H_0 is the projectile Hamiltonian, V_{0i} is the Coulomb interaction of the projectile and target electrons and H_T is the target molecule (H_2) Hamiltonian

$$H_T = H_1 + H_2 + V_{12} + 1/R. \tag{4}$$

The one-electron Hamiltonian H_i, $i = 0, 1, 2$ is given by

$$H_i = K_i - \frac{1}{|\boldsymbol{r}_i - \boldsymbol{R}/2|} - \frac{1}{|\boldsymbol{r}_i + \boldsymbol{R}/2|}, \tag{5}$$

where K_i is the kinetic energy operator.

The target states of H_2 are characterized by the orbital angular momentum projection m, spin s and parity π and are sought as an expansion in the basis of two-electron configurations

$$\Phi_n^N(x_1, x_2) = \sum_{\alpha\beta} C_{\alpha\beta}^{(n)} \phi_\alpha(\boldsymbol{r}_1)\phi_\beta(\boldsymbol{r}_2)X(s_n, v_n), \tag{6}$$

where the two-electron spin function is given by

$$X(s, v) = \sum_{\sigma_1\sigma_2} C^{sv}_{\frac{1}{2}\sigma_1\frac{1}{2}\sigma_2}\chi(\sigma_1)\chi(\sigma_2), \tag{7}$$

and $C^{lm}_{l_1m_1l_1m_2}$ is a Clebsch-Gordon coefficient.

The CI coefficients $C_{\alpha\beta}^{(n)}$ satisfy the relation $C_{\alpha\beta}^{(n)} = (-1)^{s_n} C_{\beta\alpha}^{(n)}$ to ensure the antisymmetry of the two-electron states and are obtained by diagonalization of the H_2 Hamiltonian for each target symmetry (m, s, π). The target states satisfy

$$\langle \Phi_{n'}^N | H_T | \Phi_n^N \rangle = \varepsilon_n^N \delta_{n'n}, \tag{8}$$

where ε_n^N is the energy of the state Φ_n^N.

The one-electron functions in Eq. (6) are characterized by the orbital angular momentum projection m_α and parity $\pi_\alpha = (-1)^{l_\alpha}$, and expressed as

$$\phi_\alpha(\boldsymbol{r}) = \frac{1}{r}\varphi_{k_\alpha l_\alpha}(r) Y_{l_\alpha m_\alpha}(\hat{\boldsymbol{r}}), \tag{9}$$

where the radial part is taken as the Laguerre basis functions,

$$\varphi_{kl}(r) = \sqrt{\frac{\alpha_l (k-1)!}{(k+l)(k+2l)!}} (2\alpha_l r)^{l+1} e^{-\alpha_l r} L_{k-1}^{2l+1}(2\alpha_l r). \tag{10}$$

Here α_l are the exponential fall-off parameters, L_{k-1}^{2l+1} are the associated Laguerre polynomials and k ranges from 1 to N_l, the number of functions for a given value of l.

The CCC method is a momentum-space formulation of the close-coupling approach where a set of coupled Lippmann-Schwinger equations are solved for the T-matrix

$$\langle \boldsymbol{k}_f^{(-)} \Phi_f^N | T^N | \Phi_i^N \boldsymbol{k}_i^{(+)} \rangle = \langle \boldsymbol{k}_f^{(-)} \Phi_f^N | V | \psi_i^{N(+)} \rangle, \tag{11}$$

where

$$V = V_0 + V_{01} + V_{02} + (E - H)(P_{01} + P_{02}). \tag{12}$$

The projectile electron distorted waves are solutions of

$$(\varepsilon_k - K_0 - U_0)|\boldsymbol{k}^{(\pm)}\rangle = 0 \tag{13}$$

with $\varepsilon_k = k^2/2$ and U_0 is a short-ranged central distorted potential taken as the spherically symmetric part of electron-molecule direct potential averaged over the ground state of H_2. In a similar way as it is done for electron-atom scattering [28] the Lippmann-Schwinger equations are solved by performing a partial wave expansion of the distorted waves

$$|\boldsymbol{k}^{(\pm)}\rangle = \frac{1}{k}\sum_{L,M} i^L e^{\pm i\delta_L} Y_{LM}^*(\hat{\boldsymbol{k}})|kL\rangle, \tag{14}$$

where δ_L is the distorting phase shift and the sum is taken to some maximum value of $L_{\max}$. The resulting Lippmann-Schwinger equations for the partial wave T-matrix are

$$T^{M\Pi S}_{fL_fM_f,iL_iM_i}(k_f, k_i) = V^{M\Pi S}_{fL_fM_f,iL_iM_i}(k_f, k_i) + \sum_{n=1}^{N}\sum_{L'M'}\sum\!\!\!\!\!\!\int_k dk \frac{V^{M\Pi S}_{fL_fM_f,nL'M'}(k_f, k)\, T^{M\Pi S}_{nL'M',iL_iM_i}(k, k_i)}{E^{(+)} - \varepsilon_k - \varepsilon_n^N + i0}. \tag{15}$$

Further transformation to the K-matrix formulation allows the use of real arithmetic and ensures the unitarity of the CCC approach. The equations are solved for each partial wave of the total orbital angular momentum projection M, parity Π, and spin S using standard techniques [28]. The body-frame T-matrix elements obtained from the solution of Eq. (16) are transformed into the laboratory frame and used to find cross sections for transitions of interest. In order to compare with experiment an appropriate orientation averaging of the cross sections is performed. With the definitions adopted in Ref. [48] the partial wave ICS is given by

$$\sigma_{f,i}^{M\Pi S} = \frac{q_f}{q_i}\frac{1}{4\pi}\sum_{\substack{L_f,L_i\\M_f,M_i}} |F^{M\Pi S}_{fL_fM_f,iL_iM_i}|^2, \tag{16}$$

where

$$F^{M\Pi S}_{fL_fM_f,iL_iM_i} = -(2\pi)^2(q_fq_i)^{-1}i^{L_i-L_f} \times T^{M\Pi S}_{fL_fM_f,iL_iM_i}(q_f,q_i). \quad (17)$$

and q is the linear momentum of the projectile and is used to indicate the physical T-matrix elements $T^{M\Pi S}_{fL_fM_f,iL_iM_i}(q_f,q_i)$.

The DCS analytically averaged over orientations can be expressed as

$$\frac{d\sigma^S_{fi}}{d\Omega} = \sum_j A^{Sj}_{fi} P_j(\cos\theta), \quad (18)$$

where $P_j(\cos\theta)$ is a Legendre polynomial and coefficients A^{Sj}_{fi} are given by

$$\begin{aligned} A^{Sj}_{fi} &= \frac{q_f}{q_i}\frac{1}{(4\pi)^2}\sum_{M\Pi}\sum_{\substack{L_f,L_i\\M_f,M_i}}\sum_{\substack{L'_f,L'_i\\M'_f,M'_i}}(-1)^{M'_f-M'_i}\hat{L}_i\hat{L}'_i \\ &\times\hat{L}_f\hat{L}'_f\, F^{M\Pi S}_{fL_fM_f,iL_iM_i}F^{M\Pi S*}_{fL'_fM'_f,iL'_iM'_i} \\ &\times(2j+1)^{-1}C^{j0}_{L_i0,L'_i0}C^{jM'_i-M_i}_{L_i-M_i,L'_iM'_i}C^{jM_f-M'_f}_{L_fM_f,L'_f-M'_f} \\ &\times C^{j0}_{L_f0,L'_f0}\delta_{M_i-M'_i,M_f-M'_f}. \end{aligned} \quad (19)$$

The ICS for a transition from an initial state i to the final state f in the total spin channel S is obtained as a sum over partial-wave ICS

$$\sigma^S_{fi} = \sum_{M\Pi}\sigma^{M\Pi S}_{fi}, \quad (20)$$

and spin-averaged ICS is given by

$$\sigma_{fi} = \sum_S \frac{2S+1}{2(2s_i+1)}\sigma^S_{fi}. \quad (21)$$

A similar expression holds for the spin-averaged DCS.

In the CCC method the TCS for scattering on an initial state i is given by a sum over elastic scattering and all excitation cross sections,

$$\sigma^{\rm tot}_i = \sum_f \sigma_{fi}, \quad (22)$$

while the TICS is a sum over positive energy states only

$$\sigma^{\rm ion}_i = \sum_{f:\varepsilon_f>0}\sigma_{fi}. \quad (23)$$

The convergence of the cross sections is established by increasing the size of the close-coupling expansion (1) and the size of the partial wave expansion [46].

B. Target states

We start by describing the structure models used to investigate the convergence of the close-coupling expansion. These models include a progressively larger number of states (9, 92, 259, 427, 491) and allow us to investigate the effect of various reaction channels. The use of the underlying Laguerre basis is particularly important in establishing the convergence as such a basis allows us to model both discrete and continuum spectra of the target with a finite size expansion. As the size of the Laguerre basis increases the negative energy states (relative to the H_2^+ ground state) converge to true bound states and the positive energy states provide an increasingly dense representation of the target continuum.

For some states the single-centre representation of the H_2 wave functions is slowly convergent with respect to the orbital angular momentum of the Laguerre basis. This affects the H_2 ground ($X\ ^1\Sigma_g^+$) and first excited ($b\ ^3\Sigma_u^+$) states the most, for which the multicentre effects are the strongest. We find that an effective way to deal with this issue is to produce an accurate representation of the $1s\sigma_g$ orbital of H_2^+ and use it instead of the $1s$ orbital of the Laguerre basis. This replacement also improves the accuracy of the excited states of H_2 where the frozen-core type configurations $(1s\sigma_g, nlm)$ have the dominant contribution. In the present calculations the $1s\sigma_g$ orbital was obtained by digonalization of the H_2^+ Hamiltonian in the Laguerre basis with $N_l = 60-l$, $l \le 8$, and $\alpha = 0.9$ for all l.

In order to test the convergence of the cross sections with respect to the number of states in the close-coupling expansion we have conducted calculations in five models. All models have a CI expansion that includes frozen-core configurations $(1s, nlm)$ and all $(nlm, n'l'm')$ configurations with $n, n' \le 2$. The largest model has a Laguerre basis with $N_l = 17-l$, $l \le 3$, and $\alpha_0 = 0.76$, $\alpha_1 = 0.765$, $\alpha_2 = 0.79$, and $\alpha_3 = 0.85$. These exponential fall-offs allow us to have the first positive energy state to be at approximately the same energy (0.1 eV) for all target symmetries. We find this is useful to obtain an accurate estimate of cross sections with relatively small basis size. In order to account more accurately for the electron-electron correlations in the ground state we replaced $2s$ and $2p$ Laguerre functions by short ranged Laguerre functions that have exponential fall-offs of $\alpha = 1.85$. The total number of states in this model is 491, comprising of singlet and triplet states with negative and positive parity and orbital angular momentum projection $|m| \le 3$. We will refer to this model as CCC(491). The number of negative-energy states in this model is 92. We have performed calculations using the negative energy states only and will refer to these as CC(92) model. Comparison of the CC(92) and CCC(491) results allows us to estimate the importance of coupling to ionization channels. The CC(9) model uses the first nine (seven non-degenerate) states and corresponds to previous close-coupling calculations performed for e-H_2 scattering [40, 42].

In order to check convergence with respect to the number N_l of Laguerre basis functions for a given number of orbital angular momentum we have performed calculations in the CCC(427) model that differs from the CCC(491) model only by the size of the Laguerre basis, $N_l = 15 - l$. The agreement between the results of the CCC(427) and CCC(491) models will be a good indication of the accuracy and convergence of our calculations. Finally, to check the stability of our results with respect to the maximum orbital angular momentum of the Laguerre basis we have conducted calculations in the CCC(259) model that has $N_l = 15 - l$, $l \leq 2$.

The accuracy of the target wave functions plays an important role in the establishment of the reliable theoretical collision cross sections. In Table I the two-electron and vertical excitation energies are presented for a number of low lying states of the CCC(491) model at the equilibrium internuclear distance $R_0 = 1.4$ and are compared with results of accurate calculations [56–64]. The CCC(491) structure model has negative energy states up to the principal quantum number $n = 5$ with accurate representation of the states up to the $n = 4$ shell ($B''\ ^1\Sigma_u^+$ and $D'\ ^1\Pi_u$ states). Table II presents the optical oscillator strengths (OOS) for a number of optically allowed transitions. We find a reasonably good agreement between the length and velocity forms and good agreement with previous calculations of Wolniewicz and Staszewska [62, 65]. Similarly good agreement is achieved for the ground state static dipole polarizability presented in Table III. Overall the accuracy of the CCC(491) OOS is within 10% of the accurate values and we expect that the uncertainty of the calculated cross sections due to the accuracy of the structure model will be within 10% as well.

The target wave functions in the CCC(491) and CCC(427) models are practically the same for the low-lying target states for which the excitation cross sections have been calculated, however, the CCC(259) model has somewhat less accurate representation of the negative parity states due to the omission of $l = 3$ Laguerre functions. Both CCC(427) and CCC(259) models have a less dense discretization of the continuum compared to the CCC(491) model.

TABLE I: Two-electron energy E of electronic target states of H_2 and the vertical electronic excitation energy from the ground state ΔE at the internuclear distance $R_0 = 1.4\ a_0$. Comparison is made with accurate structure calculations [56–64].

	E (a.u.)		ΔE (eV)	
State	Present	Ref.	Present	Ref.
$X\ ^1\Sigma_g^+$	-1.162	-1.174 [56]		
$b\ ^3\Sigma_u^+$	-0.770	-0.784 [57]	10.67	10.62 [57]
$a\ ^3\Sigma_g^+$	-0.710	-0.714 [58]	12.32	12.54 [58]
$c\ ^3\Pi_u$	-0.701	-0.707 [59]	12.56	12.73 [59]
$B\ ^1\Sigma_u^+$	-0.697	-0.706 [60]	12.66	12.75 [60]
$E, F\ ^1\Sigma_g^+$	-0.687	-0.692 [61]	12.92	13.13 [61]
$C\ ^1\Pi_u$	-0.683	-0.689 [62]	13.03	13.22 [62]
$e\ ^3\Sigma_u^+$	-0.640	-0.644 [63]	14.21	14.43 [63]
$h\ ^3\Sigma_g^+$	-0.628	-0.630 [64]	14.54	14.80 [64]
$d\ ^3\Pi_u$	-0.626	-0.629 [66]	14.59	14.85 [66]
$B'\ ^1\Sigma_u^+$	-0.625	-0.629 [60]	14.63	14.85 [60]
$D\ ^1\Pi_u$	-0.621	-0.624 [62]	14.74	14.99 [62]
$B''\ ^1\Sigma_u^+$	-0.600	-0.603 [60]	15.31	15.56 [60]
$D'\ ^1\Pi_u$	-0.598	-0.600 [62]	15.36	15.62 [62]

TABLE II: Oscillator strengths for transitions from the ground state to the lowest lying $^1\Sigma_u^+$ and $^1\Pi_u$ states of H_2 at the internuclear distance $R_0 = 1.4\ a_0$. Comparison is made with the calculations of Wolniewicz and Staszewska [62, 65].

Transition	Length	Velocity	Refs. [62, 65]
$X\ ^1\Sigma_g^+ \to B\ ^1\Sigma_u^+$	0.2769	0.2427	0.3013
$X\ ^1\Sigma_g^+ \to C\ ^1\Pi_u$	0.3368	0.3116	0.3579
$X\ ^1\Sigma_g^+ \to B'\ ^1\Sigma_u^+$	0.0578	0.0499	0.0575
$X\ ^1\Sigma_g^+ \to D\ ^1\Pi_u$	0.0832	0.0765	0.0848
$X\ ^1\Sigma_g^+ \to B''\ ^1\Sigma_u^+$	0.0221	0.0190	0.0210
$X\ ^1\Sigma_g^+ \to D'\ ^1\Pi_u$	0.0344	0.0317	0.0334

C. Partial wave expansion

We now turn to the convergence with respect to the partial-wave expansion. Due to the lack of spherical symmetry of the interacting potential (12) the size of the Lippmann-Schwinger equations (16) grows rapidly as the size of the partial expansion increases. To facilitate the convergence studies we have chosen to have the maximum projectile orbital angular momentum $L_{\max}$ to be equal to the maximum total orbital angular momentum $M_{\max}$ in all our calculations. In practical close-coupling calculations relatively small values of $L_{\max}$ and $M_{\max}$ have to be adopted (compared to electron-atom scattering). To verify convergence of our results with respect to the size of the partial wave expansion we have performed calculations in the CCC(259) model with $L_{\max} = 6$ while for all other models we have chosen $L_{\max} = 8$. We find that excitation of the triplet states of H_2 are well converged for the value of $L_{\max} = 6$. However, cross sections for the excitation to the singlet states at intermediate and large incident electron energies are not converged for $L_{\max} = 8$ and can be in substantial error, unless one utilizes an analytic Born subtraction (ABS) technique. In the ABS technique the extrapolated excitation ICS is obtained from

$$\sigma_{fi}^S = \sum_{M\Pi} (\sigma_{fi}^{M\Pi S} - \sigma_{fi}^{M\Pi}) + \sigma_{fi}^{\rm AB}, \qquad (24)$$

TABLE III: Static dipole polarizability (a.u.) of the ground state of H_2 at the internuclear distance $R_0 = 1.4\ a_0$ compared with the accurate results of Kolos and Wolniewicz [67].

	$\alpha_\parallel$	$\alpha_\perp$	α
CCC	6.43	4.64	5.23
Ref. [67]	6.38	4.58	5.18

where $\sigma_{fi}^{\rm AB}$ and $\sigma_{fi}^{M\Pi}$ are the orientation averaged analytical and partial-wave Born ICS [48]. We find that the partial wave expansion with $L_{\rm max} = 8$ produces convergent results in all considered transitions.

The same approach can be applied to calculate DCS. For the spin-averaged quantities we have

$$\frac{d\sigma_{fi}}{d\Omega} = \frac{d\sigma_{fi}^{\rm pw,CC}(L_{\rm max})}{d\Omega} - \frac{d\sigma_{fi}^{\rm pw,B}(L_{\rm max})}{d\Omega} + \frac{d\sigma_{fi}^{\rm AB}}{d\Omega}, \quad (25)$$

where the first and the second terms on the right-hand side are the DCS calculated with a partial wave expansion in the close-coupling method and in the Born approximation respectively, with $L_{\rm max}$ indicating the size of the expansion, and the third term represents the analytical Born DCS. In fact, the use of Eq. (25) is a standard technique to calculate DCS for electron scattering from polar molecules [68, 69]. Similarly to others [70, 71], we find that the convergence rate of (25) can be very slow for the transitions dominated by the long-range interactions, as is the case for the dipole allowed transitions (e.g. $X\ ^1\Sigma_g^+ \to B\ ^1\Sigma_u^+$) in e-$H_2$ scattering. The problem can be traced to the lack of convergence in the Born partial-wave DCS. One way to resolve this is to conduct the partial-wave first-order Born calculations (second term in Eq. (25)) to a number of partial waves $\bar{L}_{\rm max}$ sufficient to achieve reasonably convergent Born DCS. This can be verified against the analytical Born DCS. With the partial-wave Born DCS available to $\bar{L}_{\rm max}$, we need to top-up the partial-wave close-coupling DCS (first term in Eq. (25)) to the same value of $\bar{L}_{\rm max}$. In order to do this here, we prefer to conduct a small-size close-coupling calculations, for example the CC(9) model, with the required number of partial waves $\bar{L}_{\rm max}$. This produces the close-coupling DCS that are used to top-up the DCS from a larger close-coupling model (first term in Eq. (25)) from $L_{\rm max}$ to $\bar{L}_{\rm max}$. This procedure leads to well converged cross sections for the energies and transitions considered in this paper.

We illustrate the technique in Fig. 1 for the excitation of the $B\ ^1\Sigma_u^+$ state at 30 eV. The left panel in Fig. 1 presents the analytical and partial wave ($L_{\rm max} = 8$ and $\bar{L}_{\rm max} = 25$) Born DCS. The $L_{\rm max} = 8$ DCS are not converged and show large oscillations while the $\bar{L}_{\rm max} = 25$ DCS are well converged and in close agreement with the analytical Born DCS. The right panel describes the application of the ABS technique. The DCS calculated with an $L_{\rm max} = 8$ partial-wave expansion shows unphysical oscillations, which is typical for a calculation that lacks partial-wave convergence. The direct application of the ABS method in this case leads to even larger oscillations in the DCS (ABS, $L_{\rm max} = 8$), however, the top-up procedure to $\bar{L}_{\rm max} = 25$ produces a well converged cross section.

From here onwards the CCC results are calculated utilizing the ABS technique for the ICS (24) and DCS (25).

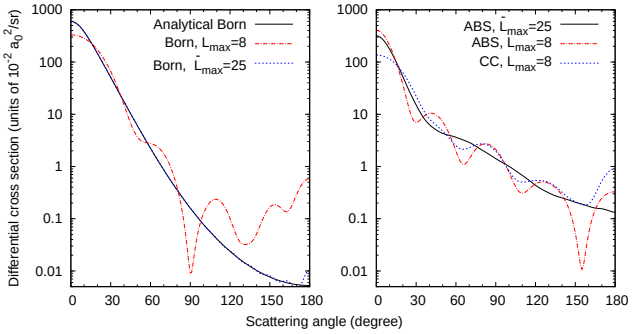

FIG. 1: Electron impact differential excitation cross section of the $B\ ^1\Sigma_u^+$ state of H_2 at 30 eV. The left panel: Analytical Born and partial-wave Born DCS with $L_{\rm max} = 8$ and $\bar{L}_{\rm max} = 25$. The right panel: close-coupling (CC) DCS for CCC(491) model with $L_{\rm max} = 8$, and ABS with $L_{\rm max} = 8$ and $\bar{L}_{\rm max} = 25$.

III. RESULTS

We have conducted close-coupling calculations of e-H_2 scattering for energies from 10 to 300 eV. As the present calculations have been performed in the FN approximation the obtained cross sections are not expected to be accurate within a few eV from the excitation thresholds. The AN approach [55] needs to be adopted at the energies close to the excitation thresholds. We have previously applied the AN approach to electron scattering from the vibrationally excited H_2^+ molecule and its isotopologues [49] and are planning to conduct similar studies for H_2 in the near future.

The present FN scattering calculations have been performed at the internuclei distance of $R_m = 1.448$. This is the average internuclei distance of the H_2 ground vibrational state. To model scattering from the ground vibrational level of H_2, the FN calculations conducted at $R_m = 1.448$ are a better approximation to the AN cross sections [72] compared to FN calculations at the equilibrium distance $R_0 = 1.40$. In Table IV the energies and OOS are presented for the CCC(491) model at the internuclei distance R_m.

No attempts have been made to map out resonance structures in the present FN calculations as they are expected to be averaged over in the more accurate AN formulation. However, the energy mesh in our calculations

TABLE IV: Two-electron energies E, the vertical excitation energies ΔE, and oscillator strengths f (length) for the electronic target states of H_2 at the internuclear distance $R_m = 1.448\ a_0$.

State	E (a.u.)	ΔE (eV)	f
$X\,^1\Sigma_g^+$	-1.161		
$b\,^3\Sigma_u^+$	-0.782	10.31	
$a\,^3\Sigma_g^+$	-0.715	12.14	
$c\,^3\Pi_u$	-0.707	12.36	
$B\,^1\Sigma_u^+$	-0.704	12.45	0.2881
$E,F\,^1\Sigma_g^+$	-0.693	12.73	
$C\,^1\Pi_u$	-0.693	12.83	0.3420
$e\,^3\Sigma_u^+$	-0.647	13.98	
$h\,^3\Sigma_g^+$	-0.634	14.34	
$d\,^3\Pi_u$	-0.632	14.39	
$B'\,^1\Sigma_u^+$	-0.631	14.42	0.0593
$D\,^1\Pi_u$	-0.627	14.54	0.0843
$B''\,^1\Sigma_u^+$	-0.606	15.10	0.0225
$D'\,^1\Pi_u$	-0.604	15.15	0.0349

is sufficiently small (0.5 eV below the ionization threshold) to verify the presence of the resonance structures predicted in the previous calculations of Branchett et al. [40] and da Costa et al. [42].

Further in this section we present cross sections for total scattering, ionization, and excitation of electronic states of H_2 calculated using five CCC models (9, 92, 259, 427 and 491 states). For the ICS we give the best estimate of the CCC results determined from the CCC(491), CCC(427) and CCC(259) cross sections. The difference between the results of these CCC models gives a good idea on the uncertainty of the cross sections and the numerical stability of the calculation. Comparison with the CC(9) and CC(92) results indicates the importance of coupling to high-lying excited states and ionization channels.

Many other calculations have been performed for e-H_2 excitation cross sections. We compare here with DW calculations of [37–39] and the largest available close-coupling calculations performed using RMPS [43], RM [40, 41], and SMC [42] methods. A detailed comparison between the earlier close-coupling calculations can be found in Ref. [42].

In comparison with the experimental results we concentrate predominately on the measurements of DCS and the ICS derived from them. Measurements of optical excitation functions are also available for many states of H_2. These measurements are affected by cascades from the upper levels which were hard to quantify accurately. We have chosen not to renormalize the available relative cross sections in order to make clear the level of agreement between our results and generally accepted cross sections values. Finally, we will also compare with the recommended data-set as suggested by Yoon et al. [1].

A. Total and ionization cross sections

In Fig. 2 we present the TCS for electron scattering from the ground state of H_2. The left panel demonstrates the convergence of our results. The three largest models agree well over the 10 to 300 eV range, however the results of the CC(92) and CC(9) models are substantially lower. This is a typical situation in electron scattering from atoms and molecules and can be explained by significantly low values of the static dipole polarizability in the CC(92) and CC(9) models; see Table V. In fact more than 30% of the polarizability comes from the continuum spectrum of H_2. This suggests that coupling to ionization channels is particularly important. The right panel presents our best estimate of the CCC cross section determined from the CCC(491), CCC(427), and CCC(259) results, and is compared with available experimental data [5–11, 73]. There is a good agreement between all experimental results and present calculations. The recommended data of Yoon et al. [1] (not shown) are practically identical with the CCC results.

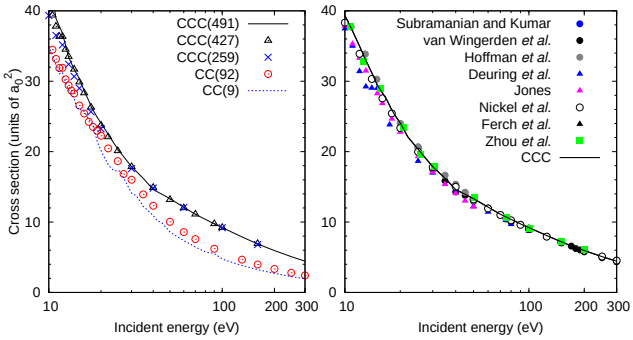

FIG. 2: Total cross section of electron scattering from the ground state of H_2. The left panel presents convergence studies for the CCC models described in the text and the right panel presents the comparison with the measurements of Subramanian and Kumar [10], van Wingerden et al. [6], Hoffman et al. [7], Deuring et al. [8], Jones [9], Nickel et al. [11], Ferch et al. [5], and Zhou et al. [73].

TABLE V: Static dipole polarizability (a.u.) of the ground state of H_2 for a number of the calculation models at the internuclear distance $R_m = 1.448\ a_0$.

Model	$\alpha_\parallel$	$\alpha_\perp$	α
CCC(491)	6.79	4.81	5.47
CCC(427)	6.78	4.81	5.46
CCC(259)	6.67	4.78	5.41
CC(92)	5.16	3.07	3.77
CC(9)	4.13	2.30	2.91

In Fig. 3 we present the single ionization cross sections. With good agreement between CCC(491), CCC(427),

and CCC(259) models we demonstrate convergence of our results across all energies. Experimental data exists for TICS [2, 74] and the H_2^+ production cross section [75, 76] that differ by the dissociative ionization cross section which is small ($< 1.5\%$). Our results are in very good agreement with experimental data and in good agreement with previous RMPS [43] and TDCC [44] calculations. The RMPS results are available from the ionization threshold to 30 eV. An averaging procedure was used in the RMPS calculatons to smooth over the pseudoresonance behavior. The final RMPS cross section is practically indistinguishable from the CCC results, which require no averaging over pseudoresonances. The TDCC results are available at 25, 50 and 75 eV. They are obtained within the one-electron and local-exchange approximations, nevertheless the agreement with CCC is good. The agreement with the recommended data of Yoon et al. [1] is good, though, our results are about 4% larger at high energies.

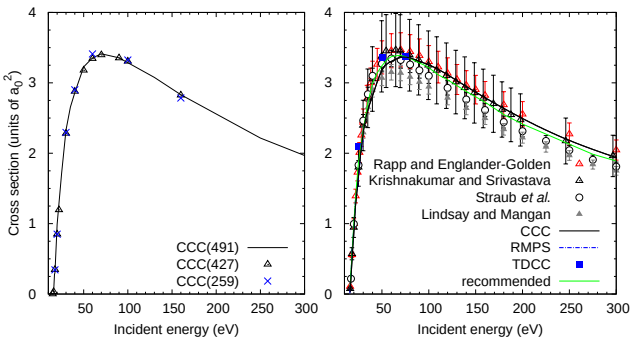

FIG. 3: Ionization cross section for electron scattering from the ground state of H_2. The left panel presents convergence studies for the CCC models described in the text and the right panel presents the comparison with the measurements of Rapp and Englander-Golden [74], Krishnakumar and Srivastava [75], Straub et al. [76], and Lindsay and Mangan [2], and calculations of Gorfinkiel and Tennyson [43] (RMPS) and Pindzola et al. [44] (TDCC), and the recommended data of Yoon et al. [1].

B. Excitation to triplet states

The ICS for the $b\ ^3\Sigma_u^+$ state are presented in Fig. 4. The CCC(491), CCC(427), and CCC(259) results are in good agreement over the entire 10–60 eV energy range. At low energies (< 15 eV) the CC(9) and CC(92) results are practically the same as the larger CCC models, however, as the incident energy increases above the ionization threshold the CC(9) and CC(92) models start to systematically overestimate the cross section. The CC(9) model shows a pseudo-resonance behavior which is characteristic for a small close-coupling calculation. Similar but significantly more pronounced pseudo-resonance structures can also be seen in the right panel of Fig. 4 for the RM [41] and SMC [42] calculations and to a lesser degree for the RMPS results [43]. None of the previous close-coupling calculations are converged for this transition but the largest RMPS results seems to be oscillating around the CCC cross section for energies above 15 eV. The DW cross sections [38] are significantly larger than present results for all energies.

Comparing with the experiments we find very good agreement at low energies but at higher energies (≥ 15 eV) the experimental results are substantially larger and seem to predict a broad maximum at around 15 eV while the CCC result exhibits a sharp maximum at the energies closer to the excitation threshold. Such behavior of the CCC cross section is consistent with the behavior of the cross sections for the triplet state excitation in e-He scattering [51]. The recommended data of Yoon et al. [1] follow the experimental values of Khakoo and Segura [13] and Khakoo et al. [14] and are in substantial disagreement with the CCC results.

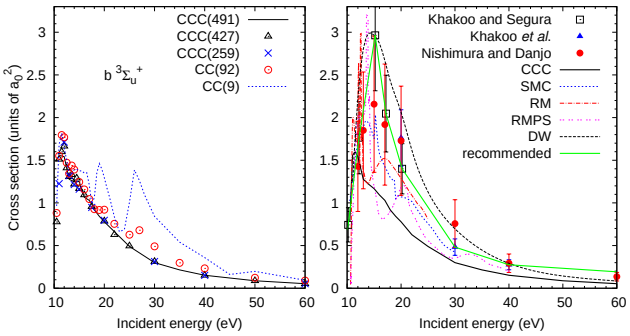

FIG. 4: Electron impact excitation cross section of the $b\ ^3\Sigma_u^+$ state of H_2. The left panel presents convergence studies for the CCC models described in the text and the right panel presents the comparison with the measurements of Khakoo et al. [14], Nishimura and Danjo [15], and Khakoo and Segura [13], and calculations of da Costa et al. [42] (SMC), Branchett et al. [40] (RM), Gorfinkiel and Tennyson [43] (RMPS), and Fliflet and McKoy [38] (DW), and the recommended data of Yoon et al. [1].

DCS for the $b\ ^3\Sigma_u^+$ state are presented in Fig. 5 at 12, 13, 15 eV and in Fig. 6 for 17.5, 20, 30 and 60 eV and compared with available experimental data [13–16], and RM [41], SMC [42], and DW [37, 38] calculations. At low energies (12-15 eV) the DCS have a pronounced peak at backward angles which is well reproduced in all our calculations, the SMC and DW calculations, and the experiment but not in the RM calculation. It is likely that the RM calculations have been affected by an error in the accounting of the phase factors [77]. As the incident electron energy increases the DCS become progressively more flat and then a peak starts to develop at around 30 degrees. With the increase of energy above 15 eV the smaller CC(9) and CC(92) calculations yield substantially larger cross sections than the CCC(491), CCC(427), and CCC(259) calculations that include coupling to ionization channels. This is consistent with the expected effects of strong interchannel coupling for ex-

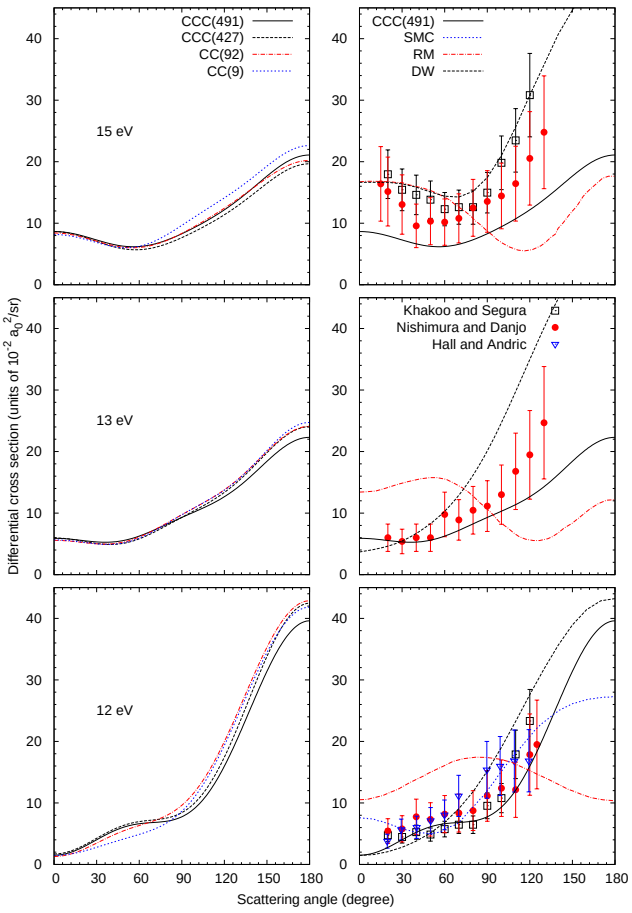

FIG. 5: Electron impact differential excitation cross section of the $b\ ^3\Sigma_u^+$ state of H_2 at 12, 13, and 15 eV. The left panel presents convergence studies for the CCC models described in the text and the right panel presents the comparison with the measurements of Khakoo and Segura [13] (performed at 12.2 and 15.2 eV), Nishimura and Danjo [15], and Hall and Andric [16], and calculations of Branchett et al. [41] (RM), da Costa et al. [42] (SMC), Fliflet and McKoy [38] at 12 and 15 eV and Rescigno et al. [37] at 13 eV (DW).

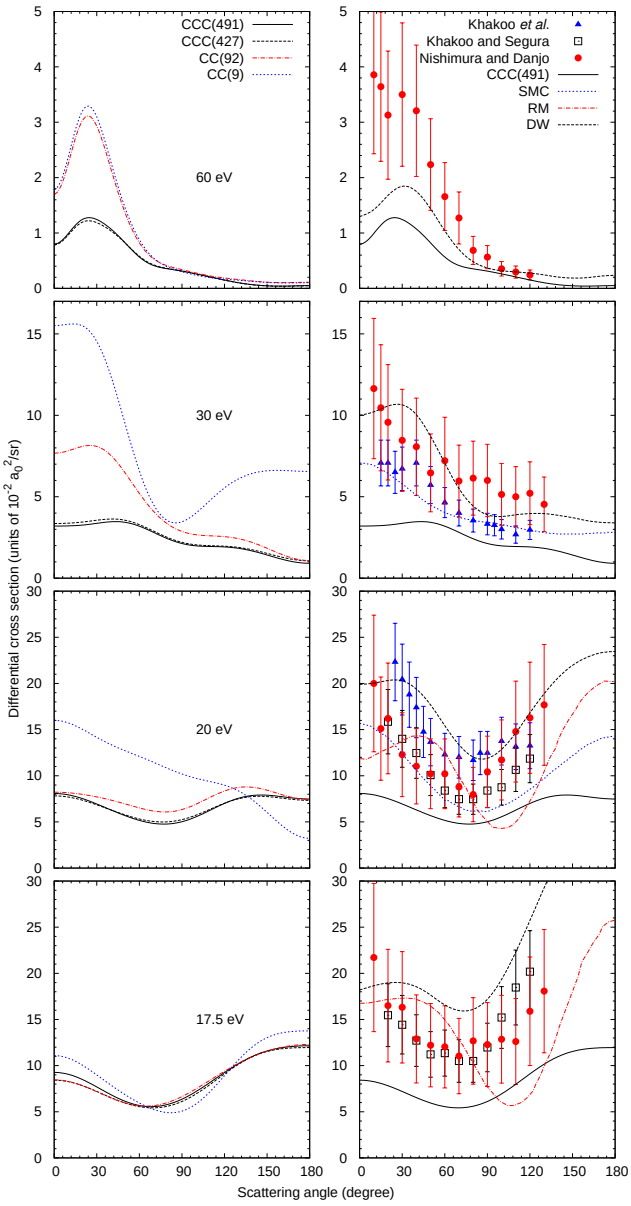

FIG. 6: Same as in Fig. 5 but at 17.5, 20, 30, and 60 eV. The experiment of Khakoo et al. [14], RM [41] and DW [37] calculations were performed at 17 eV and presented in the 17.5 eV panel. The DW calculations of Fliflet and McKoy [38] are presented at 20, 30, and 60 eV.

change dominated transitions. Similarly and for the same reasons, SMC and DW cross sections are substantially larger than the CCC DCS at these energies. Our calculations are in good agreement with the shape of the experimental DCS but are systematically lower for energies above 15 eV. As the experimental ICS have been obtained by integration over measured DCS the disagreement in the absolute values is the same as for ICS.

As we mentioned at the start of this Section, the present FN results could be inaccurate at energies close to the excitation threshold. The AN cross sections for the $b\ ^3\Sigma_u^+$ state have been calculated using the above mentioned RM 9-state method [78]. The major difference from the FN results is the flattening of the cross section peak and extension of the cross section to lower energies. We found a similar effect in our AN calculations of e-H_2^+ scattering [48] at low energies, but only minor differences between the AN and FN cross sections at larger energies. These suggest that the disagreement between the present CCC results and experiment for energies larger than 15 eV is unlikely to be due to the inaccuracy of the FN approximation and deserve further investigation.

In Fig. 7 the ICS for the $a\ ^3\Sigma_g^+$ state are presented. All our models predict a sharp rise of the cross section at the excitation threshold. We find good convergence of the CCC calculations. Like in the $b\ ^3\Sigma_u^+$ excitation ICS, the CC(92) model starts to overestimate the cross section at energies above the ionization threshold. The

CC(9) model shows a different energy dependence at low energies and has substantially larger cross sections over the entire energy range. The RM [41] and SMC [42] calculations show strong resonance structures. For energies above the ionization threshold the RM, SMC, and DW [37] results are substantially larger than the CCC results. We find very good agreement with the experiment of Wrkich et al. [18] at 17.5 and 30 eV but not at 20 eV. In our opinion it is highly unlikely that the cross section for this exchange transition is rising from 17.5 to 20 eV, noting that all vibrational bound states are open by approximately 15 eV. The experiment of Khakoo and Trajmar [17] shows the same energy dependence of the cross section as our results but are higher in magnitude. Yoon et al. [1] took the data of Wrkich et al. [18] as recommended. We have also presented the electron excitation function measurements of Ajello and Shemansky [25]. These relative cross sections have been normalized to the ICS of Khakoo and Trajmar [17] at 20 eV and could be affected by cascades. Similar to the CCC results, their cross section shows a sharp rise at the threshold with the peak at 16 eV. For the DCS in Fig. 8 the CCC results are a significant improvement over previous RM, SMC, and DW calculations. At 30 eV our calculations seems to favor the experiment of Wrkich et al. [18] rather than Khakoo and Trajmar [17]. However the first two points of the Wrkich et al. [18] DCS show a sharp rise at forward angles which is rather unusual for an exchange transition and is not supported by our calculations.

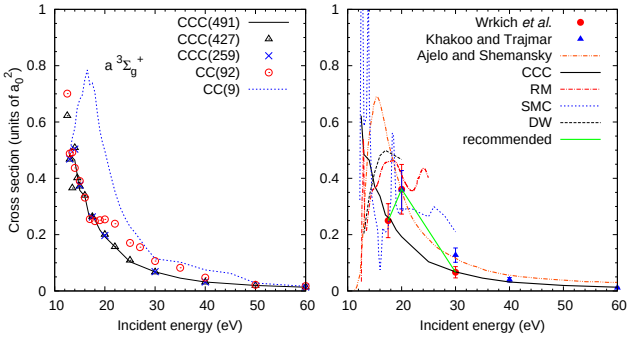

FIG. 7: Electron impact excitation cross section of the $a\ ^3\Sigma_g^+$ state of H_2. The left panel presents convergence studies for the CCC models described in the text and the right panel presents the comparison with the measurements of Khakoo and Trajmar [17], Wrkich et al. [18], and Ajello and Shemansky [25], and calculations of Branchett et al. [41] (RM), da Costa et al. [42] (SMC), and Rescigno et al. [37] (DW), and the recommended data of Yoon et al. [1].

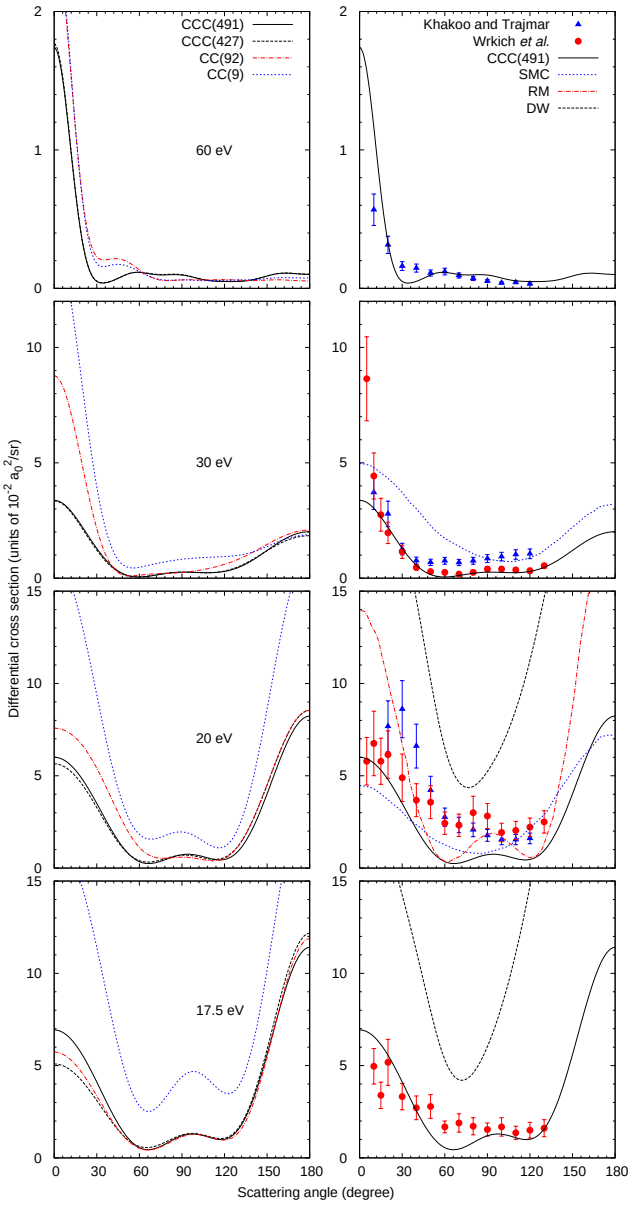

FIG. 8: Electron impact differential excitation cross section of the $a\ ^3\Sigma_g^+$ state of H_2 at 17.5, 20, 30, and 60 eV. The left panel presents convergence studies for the CCC models described in the text and the right panel presents the comparison with the measurements of Khakoo and Trajmar [17] and Wrkich et al. [18], and calculations of Branchett et al. [41] (RM), da Costa et al. [42] (SMC), and Rescigno et al. [37] (DW).

Cross sections for the excitation of the $c\ ^3\Pi_u$ state are presented in Fig. 9 for the ICS and Fig. 10 for DCS at 17.5, 20, 30, and 60 eV. The situation here is practically the same as for the $a\ ^3\Sigma_g^+$ state. We find good agreement between the CCC(491), CCC(427), and CCC(259) models for both the ICS and DCS. The smaller CC(9) and CC(92) models and RM and SMC calculations show strong resonance behavior and overestimate the cross section above the ionization threshold as seen in Fig. 9 for the ICS. We note very good agreement with the experiment of Wrkich et al. [18] at 17.5 eV but not at 20 and 30 eV. At 20 eV the experimental ICS and DCS are larger than CCC results by more than a factor of two though the shape of the DCS is similar. At 30 eV both experimental DCS of Khakoo and Trajmar [17] and Wrkich et al. [18] show a strong rise for the forward scattering angles that is absent in our two largest models. However

at 60 eV we find good agreement with the experiment of Khakoo and Trajmar [17] at the cross section peak at around 20 degrees. The ICS recomended by Yoon et al. [1] follow the Wrkich et al. [18] cross sections. We have also presented the relative excitation function measurements of [22] that were normalized at 20 eV to the ICS value of Khakoo and Trajmar [17] as given by Brunger and Buckman [3]. These data show a similar shape to the CCC cross sections but are about twice the magnitude in absolute values.

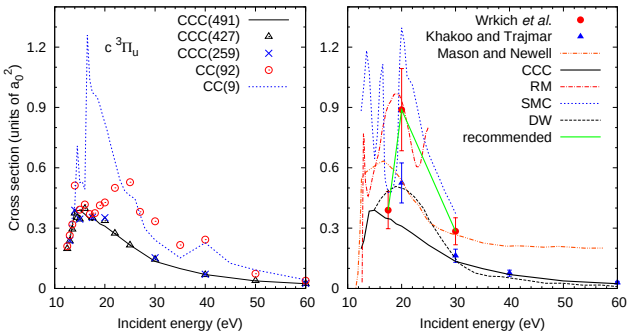

FIG. 9: Electron impact excitation cross section of the $c\ ^3\Pi_u$ state of H_2. The left panel presents convergence studies for the CCC models described in the text and the right panel presents the comparison with the measurements of Khakoo and Trajmar [17], Wrkich et al. [18], and Mason and Newell [22], and calculations of Branchett et al. [41] (RM), da Costa et al. [42] (SMC), and Mu-Tao et al. [39] (DW), and the recommended data of Yoon et al. [1].

We present in Fig. 11 and Fig. 12 the ICS and DCS for the $e\ ^3\Sigma_u^+$ state, and the ICS for the $h\ ^3\Sigma_g^+$ and $d\ ^3\Pi_u$ states in Fig. 13. There are no previous calculations for these states but experimental data is available for the $e\ ^3\Sigma_u^+$ state. For these high-lying states the excitation cross section becomes small and is strongly affected by the inter-channel coupling as can be seen by the difference between the CC(92) model and our two larger models. Numerical instabilities can be an issue for weak transitions and is the case for the $e\ ^3\Sigma_u^+$ state, where the largest CCC(491) model suffers a loss of accuarcy and/or pseudoresonance behavior for energies below 20 eV. We choose more smooth CCC(427) and CCC(259) results as preferable in this case. Comparing the experimental DCS of Wrkich et al. [18] with our results we note that our 20 and 30 eV DCS for the $e\ ^3\Sigma_u^+$ state do not show a sharp rise at small scattering angles that is seen in the experimental data. At 17.5 eV our DCS are substantially larger than the experiment which translates into larger ICS values. The drop in the measured ICS from 20 to 17.5 eV is not supported by our calculations that show a smooth rise to the threshold. Similar energy behavior is found for the $h\ ^3\Sigma_g^+$ and $d\ ^3\Pi_u$ state ICS; see Fig. 13.

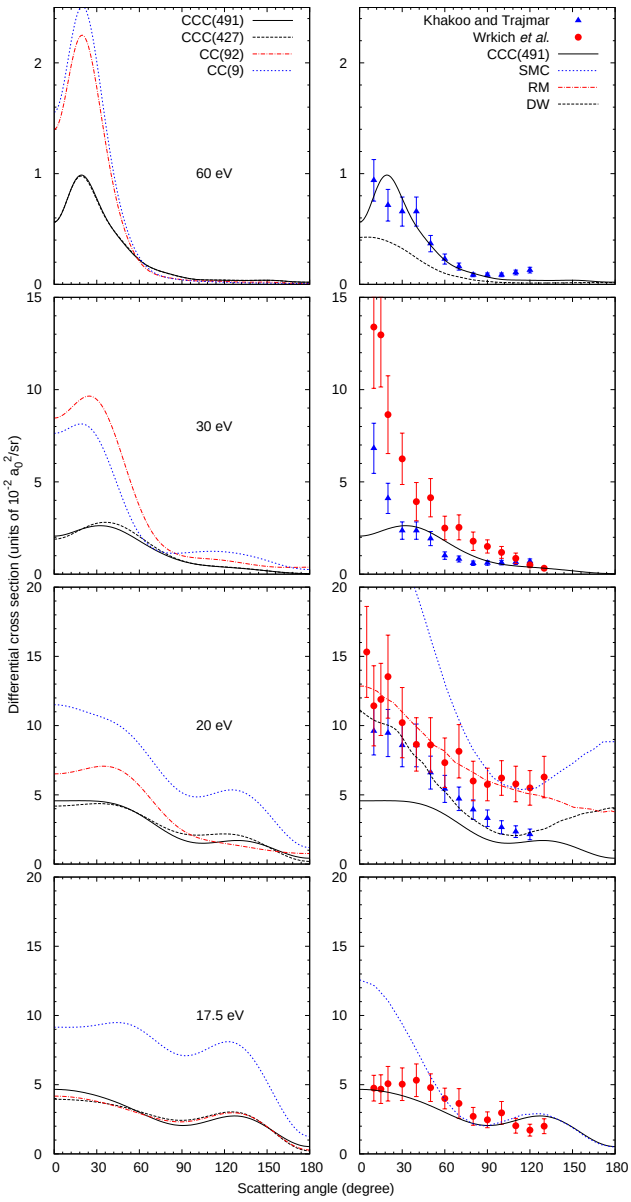

FIG. 10: Electron impact differential excitation cross section of the $c\ ^3\Pi_u$ state of H_2 at 17.5, 20, 30, and 60 eV. The left panel presents convergence studies for the CCC models described in the text and the right panel presents the comparison with the measurements of Khakoo and Trajmar [17] and Wrkich et al. [18], and calculations of Branchett et al. [41] (RM), da Costa et al. [42] (SMC), and Mu-Tao et al. [39] (DW).

C. Excitation to singlet states

We now turn to the excitation of the singlet states of H_2. In addition to our five close-coupling models we have also presented the cross sections obtained from the first-order Born calculations. Comparison with the Born results indicates the importance of the close-coupling effects and establishes the energy region where these effects

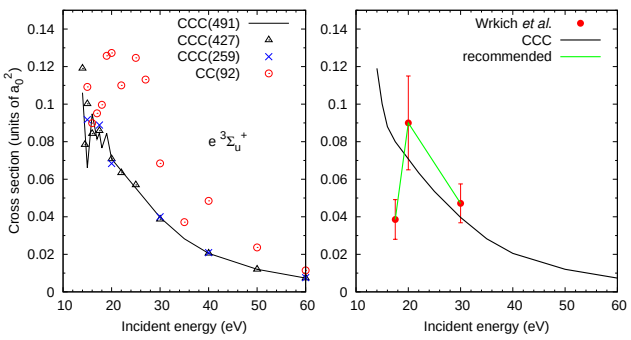

FIG. 11: Electron impact excitation cross section of the $e\ ^3\Sigma_u^+$ state of H_2. The left panel presents convergence studies for the CCC models described in the text and the right panel presents the comparison with the measurements of Wrkich et al. [18] and the recommended data of Yoon et al. [1].

become insignificant. For all singlet-state excitations we find very good agreement between our largest CCC(491) and CCC(427) models and are confident in establishing convergent results. The CCC(259) model cross sections are found to be marginally larger for the optically allowed transitions at the cross section peak. This is mostly due to the smaller projectile partial wave expansion in the CCC(259) model ($L_{\max} = 6$) as compared to the CCC(491) and CC(427) models ($L_{\max} = 8$). The ABS procedure is not quite converged yet for $L_{\max} = 6$.

In Fig. 14 and Fig. 15 the ICS and DCS for the $E, F\ ^1\Sigma_g^+$ state are presented. We find a very large reduction in the ICS from the Born and CC(9) values to the converged CCC results. The latter predicts a nearly flat, slowly decreasing cross section from the threshold to high energy. Comparing with the Born ICS we find that the close-coupling effects seems to be important up to 300 eV. The SMC cross sections of da Costa et al. [42] show a strong resonance behavior at threshold and at about 18 eV, which is absent in our converged results but is similar to the CC(9) model behavior. The RM calculations of Branchett et al. [41] increase rapidly from the threshold and do not show any resonances. The RM cross section values are significantly larger than those from the CCC calculations and the SMC results. Comparing with the experiment of Wrkich et al. [18] we find good agreement at all three available energies. Results derived from the emission measurements of Liu et al. [80] are recommended for this transition by Yoon et al. [1] and are in good agreement with the CCC calculations and experiment of Wrkich et al. [18]. A more detailed comparison with experimental DCS reveals a near perfect agreement at 30 eV and good agreement at 17.5 eV. At 20 eV the CCC results predict a flat cross sections at around 90 degrees while the experiment and SMC results show a local maximum. At this energy the shape of the RM results is very similar to the CCC DCS however the absolute values are more than ten times larger. At all three energies the experimental DCS show a strong rise at forward

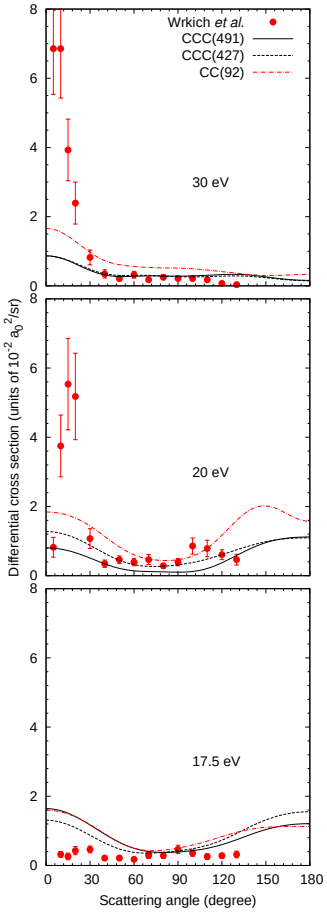

FIG. 12: Electron impact differential excitation cross section of the $e\ ^3\Sigma_u^+$ state of H_2 at 17.5, 20, and 30 eV. Convergence studies are presented for the CCC models described in the text. Measurements are due to Wrkich et al. [18].

scattering angles in agreement with the CCC results.

Cross sections for optically allowed transitions from the ground state to the $B\ ^1\Sigma_u^+$, $C\ ^1\Pi_u$, $B'\ ^1\Sigma_u^+$, $D\ ^1\Pi_u$, $B''\ ^1\Sigma_u^+$, and $D'\ ^1\Pi_u$ states are presented in Figs. 16-25. The ICS for these transitions have a similar shape with a broad maximum at around 70 eV. The high energy ICS for optically allowed transitions are predetermined by the value of the OOS [81] which are sufficiently accurate in the present calculations. For all transitions we find that the Born ICS converge to the CCC results at around 300 eV and have a maximum at around 30-40 eV. At lower energies the Born and small close-coupling models overestimate the cross sections, particularly for the high-lying states. The CC(9) model proved to be particularly poor with significant lack of convergence already at 17.5 eV as can be seen from the analysis of the DCS convergence in Figs. 17 and 21. Similar to our CC(9) model the RM and SMC cross sections for the $B\ ^1\Sigma_u^+$ and $C\ ^1\Pi_u$ states rise sharply at the threshold and are significantly larger than the converged CCC cross sections.

The ICS for the $B\ ^1\Sigma_u^+$ state presented in Fig. 16 show good agreement with the experiments of Kato et al. [20]

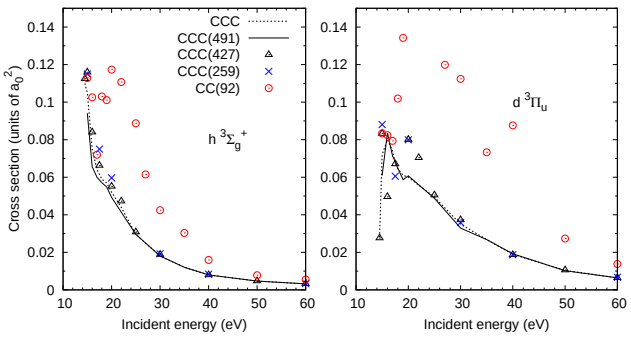

FIG. 13: Electron impact excitation cross sections of the $h\ ^3\Sigma_g^+$ and $d\ ^3\Pi_u$ states of H_2. Convergence studies are presented for the CCC models described in the text. Measurements are due to Mohlmann and de Heer [79].

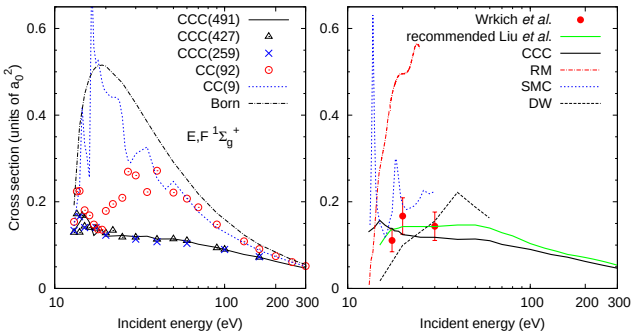

FIG. 14: Electron impact excitation cross section of the $E, F\ ^1\Sigma_g^+$ state of H_2. The left panel presents convergence studies for the CCC models described in the text and the right panel presents the comparison with the measurements of Wrkich et al. [18] and Liu et al. [80], and calculations of Branchett et al. [41] (RM), da Costa et al. [42] (SMC), and Mu-Tao et al. [39] (DW), and the recommended data of Yoon et al. [1].

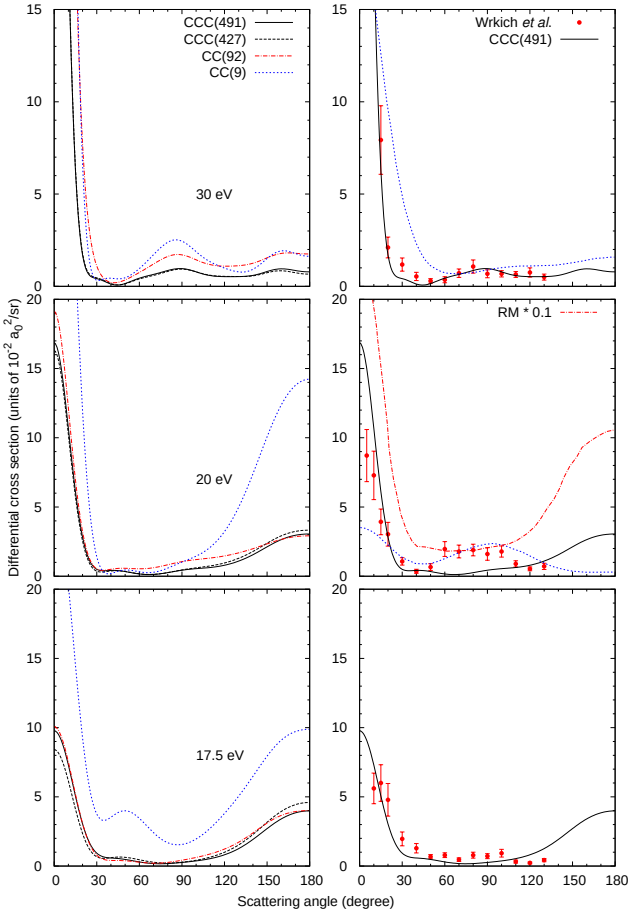

FIG. 15: Electron impact differential excitation cross section of the $E, F\ ^1\Sigma_g^+$ state of H_2 at 17.5, 20, and 30 eV. The left panel presents convergence studies for the CCC models described in the text and the right panel presents the comparison with the measurements of Wrkich et al. [18] and calculations of Branchett et al. [41] (RM) and da Costa et al. [42] (SMC).

and Khakoo and Trajmar [17] while the data of Wrkich et al. [18] are too large and the data of Srivastava and Jensen [19] become smaller than the CCC results above 30 eV. Yoon et al. [1] chose the data obtained from the optical excitation function measurements of Liu et al. [23] as recommended. The agreement between different experiments is reasonably good. The CCC calculations agree with the recommended data at high energies, however the peak of the cross section in the recommended data is at lower energies and the absolute value of the cross section at the peak is lower by 5%. The $B\ ^1\Sigma_u^+$ state DCS are presented at 17.5, 20, 30, 40, 60, 100, and 200 eV in Figs. 17-19 and are compared with the experiments of Kato et al. [20], Wrkich et al. [18], and Khakoo and Trajmar [17] and RM [41], SMC [42], and DW [38] calculations. The CCC results for the $B\ ^1\Sigma_u^+$ state DCS are in very good agreement in shape and absolute values with the experiment at 17.5 eV and are a significant improvement over the SMC results. At 20 eV the forward scattering DCS are nearly half the magnitude of the experimental values of Wrkich et al. [18] but are closer to the data of Khakoo and Trajmar [17]. The SMC forward scattering DCS at 20 eV is in good agreement with the CCC results, but at greater scattering angles the SMC results become substantially larger. At 30 eV the disagreement for the forward scattering angles with the experiment of Wrkich et al. [18] becomes substantially smaller and we also find good agreement with the experiment of Khakoo and Trajmar [17]. As the incident energy increases the DCS becomes highly peaked in the forward direction. At 40, 60, 100, and 200 eV we find a very good agreement with the forward scattering DCS data of Kato et al. [20] and Khakoo and Trajmar [17]. However, at intermediate and large scattering angles our results are systematically lower than the experiment of Khakoo and Trajmar [17]. Surprisingly, at 40 and 60 eV the DW results [38] are in much better agreement with the experiment of Khakoo and Trajmar [17] at larger scattering angles.

For the $C\ ^1\Pi_u$ state the comparison of the CCC DCS

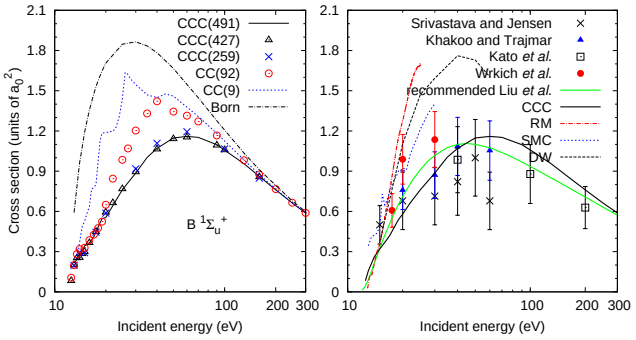

FIG. 16: Electron impact excitation cross section of the $B\ ^1\Sigma_u^+$ state of H_2. The left panel presents convergence studies for the CCC models described in the text and the right panel presents the comparison with the measurements of Khakoo and Trajmar [17], Srivastava and Jensen [19], Liu et al. [23], Wrkich et al. [18], and Kato et al. [20], and calculations of Branchett et al. [41] (RM), da Costa et al. [42] (SMC), and Fliflet and McKoy [38] (DW), and the recommended data of Yoon et al. [1].

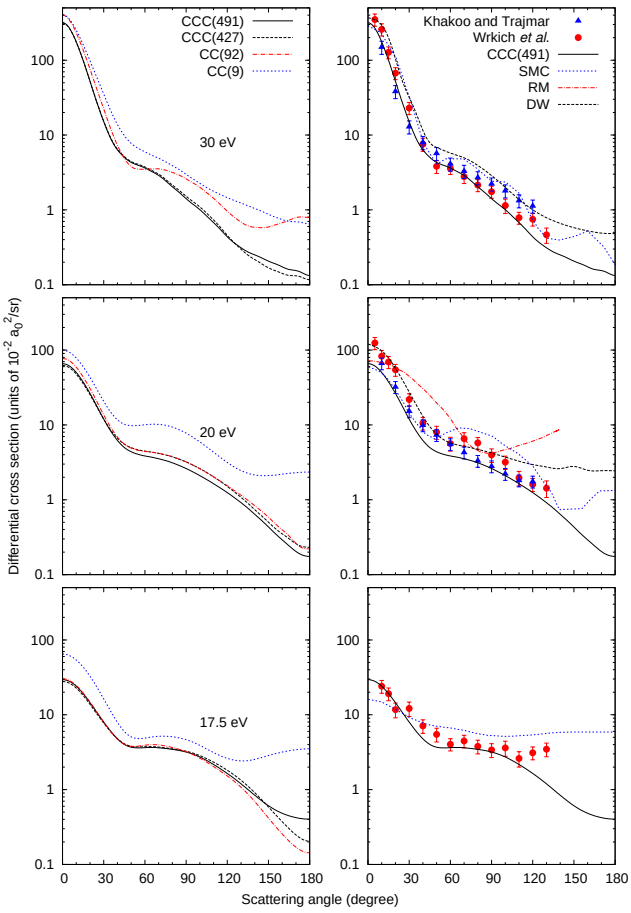

FIG. 17: Electron impact differential excitation cross section of the $B\ ^1\Sigma_u^+$ state of H_2 at 17.5, 20, and 30 eV. The left panel presents convergence studies for the CCC models described in the text and the right panel presents the comparison with the measurements of Wrkich et al. [18] and Khakoo and Trajmar [17], and calculations of Branchett et al. [41] (RM), da Costa et al. [42] (SMC), and Fliflet and McKoy [38] (DW).

with the experiment is presented at 17.5, 20 and 30 eV in Fig. 21 and it mirrors what we discussed above for the $B\ ^1\Sigma_u^+$ state. At larger energies the situation is somewhat different; see Figs. 22 and 23. At 40 eV the CCC DCS are in much better agreement with measurements of Kato et al. [20] at 20 and 30 degrees while measurements of Khakoo and Trajmar [17] are nearly twice as low. The value for the OOS for this state obtained in our calculation (0.342) is in agreement with the OOS (∼0.34) obtained by accurate theory [82–84] and measurements [85–87] but differs substantially with the estimate (0.226) obtained from the DCS measurements of Kato et al. [20]. This translates to much smaller experimental ICS as can be seen in Fig. 20 at 100 and 200 eV. Similar to the $B\ ^1\Sigma_u^+$ state, Yoon et al. [1] chose the data of Liu et al. [23] as recommended. The agreement between experimental results is relatively good. Our calculations differ substantially from the recommended data. At the peak of the cross section our results are larger by 18% and clearly have larger high energy asymptotic values.

We present ICS for the $B'\ ^1\Sigma_u^+$ and $D\ ^1\Pi_u$ states in Fig. 24 and those for the $B''\ ^1\Sigma_u^+$ and $D'\ ^1\Pi_u$ states in Fig. 25, and compare with the data derived from emission cross section measurements by Liu et al. [26] and Glass-Maujean et al. [27]. For all these states the CCC cross sections are substantially larger at high energies.

IV. CONCLUSIONS

We have reported detailed convergence studies for electron-impact excitation cross sections of electronic states, total scattering and total ionization cross sections in the energy range from 10 to 300 eV. We find that calculations performed in the CC(9) model are insufficient for practically all transitions and considered energies except for the excitation of the $b\ ^3\Sigma_u^+$ state at 10 to 15 eV. The previous RM [40, 41] and SMC [42] calculations have the same size close-coupling expansion as in our CC(9) model and produce cross sections that exhibit a similar lack of convergence. Comparison of fully converged CCC results with the CC(92) model that has only the bound states in the close-coupling expansion allows us to signify the importance of the coupling to the ionization channels. For energies above the ionization threshold such coupling proved to be important. This finding is consistent with the fact that more than 30% of the static dipole polarizability of the H_2 ground state comes from the continuum part of the spectrum.

The uncertainty estimates are increasingly becoming a standard requirement in presenting theoretical results [88]. The use of the collisions data in plasma modeling makes an estimate of the accuracy of the collision data particularly important [89]. The uncertainty of the CCC results can be estimated by comparing cross sections ob-

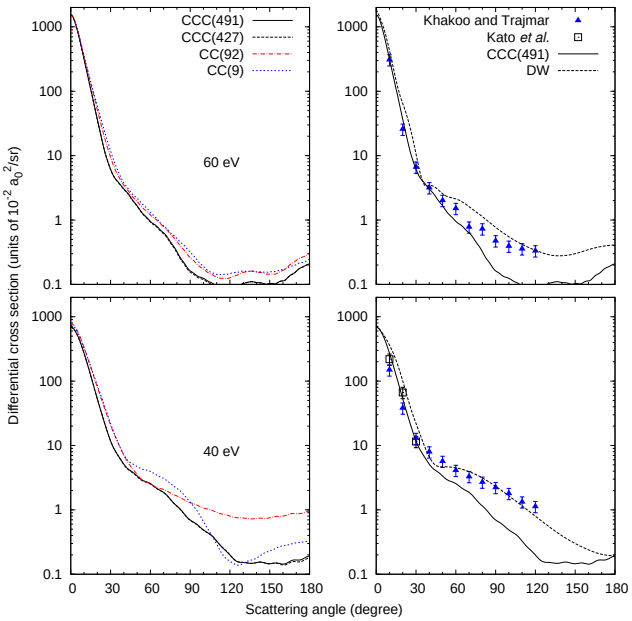

FIG. 18: Same as in Fig. 17 but at 40 and 60 eV. In addition the measurements of Kato et al. [20] are also presented.

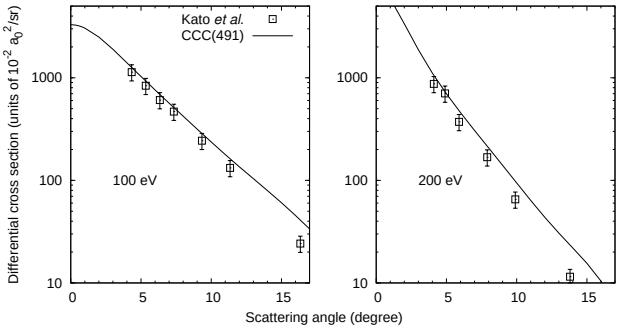

FIG. 19: Same as in Fig. 18 but at 100 and 200 eV.

tained in CCC(491), CCC(427), and CCC(259) models. Practically for all considered cross sections we find a very good rate of convergence which we estimate to be better than 5%. Combining this with the accuracy of the collision data due to the H_2 structure model (10%) we believe that the overall uncertainty of the presented cross sections is better than 11%. We should stress, though, that this uncertainty estimate is within the FN approximation. For energies close to the excitation thresholds the FN cross sections are likely to be inaccurate. This should affect the triplet state cross sections more than singlet ones as the former have a sharp rise near threshold. The AN approach has to be applied at these energies to attain a reliable estimate.

For a number of electronic excitations we find significant differences between the converged CCC cross sections and experiment. For the $b\ ^3\Sigma_u^+$ state our ICS are substantially lower than experimental values above 15 eV. For all triplet state excitation ICS our results predict

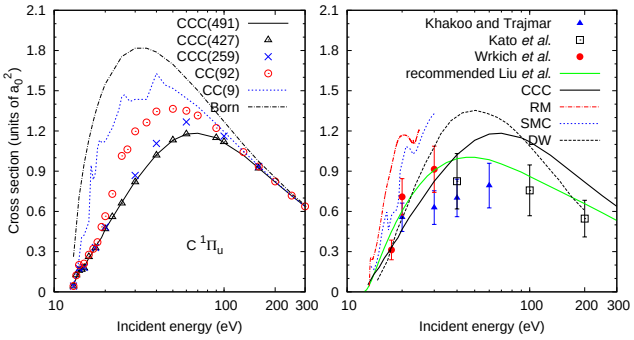

FIG. 20: Electron impact excitation cross section of the $C\ ^1\Pi_u$ state of H_2. The left panel presents convergence studies for the CCC models described in the text and the right panel presents the comparison with the measurements of Khakoo and Trajmar [17], Wrkich et al. [18], Kato et al. [20], and Liu et al. [23], and calculations of Branchett et al. [41] (RM), da Costa et al. [42] (SMC), and Mu-Tao et al. [39] (DW), and the recommended data of Yoon et al. [1].

a sharp rise at the excitation threshold and then a smooth decrease with increasing incident electron energy. This is in disagreement with measurements of Wrkich et al. [18] for the $a\ ^3\Sigma_g^+$, $c\ ^3\Pi_u$, and $e\ ^3\Sigma_u^+$ states, which seem to predict a much more gradual increase. For a number of energies and triplet state DCS we find that the sharp rises measured at forward scattering angles are not supported by the CCC calculations and perhaps artifacts of the unfolding procedure in the experimental analysis.

Excitation to the $E, F\ ^1\Sigma_g^+$ state shows a dramatic effect of inter-channel coupling that leads to a significantly smaller and nearly flat ICS that is in good agreement with the experiments of Liu et al. [80] and Wrkich et al. [18]. For optically allowed transitions the inter-channel effects are not as dramatic as for the $E, F\ ^1\Sigma_g^+$ state, but are still very important to achieve accurate cross sections. For the $C\ ^1\Pi_u$ state our calculations support the OOS (∼0.34) obtained by accurate theory [82–84] and measurements [85–87] rather than OOS value of 0.226 obtained via DCS measurements by Kato et al. [20].

Comparing with recommended e-H_2 excitation cross sections suggested by Yoon et al. [1] we find substantial differences for all triplet state excitations. For excitations to the singlet states we find good agreement for the $E, F\ ^1\Sigma_g^+$ and $B\ ^1\Sigma_u^+$ states but not for the $C\ ^1\Pi_u$ state. We also find substantial differences with the excitation cross sections derived from the measurement of the emissions cross sections [26, 27] for the $B'\ ^1\Sigma_u^+$, $D\ ^1\Pi_u$, $B''\ ^1\Sigma_u^+$, and $D'\ ^1\Pi_u$ states.

The e-H_2 cross sections presented here are the first set of theoretical cross sections for this scattering system that are explicitly demonstrated to be convergent and cover a large energy region from the threshold to 300 eV. These results will be made available via LXCat database [90] and we hope will be useful in various applications.

In the near future we are planning to investigate the effect of nuclear motion on e-H_2 cross sections using a

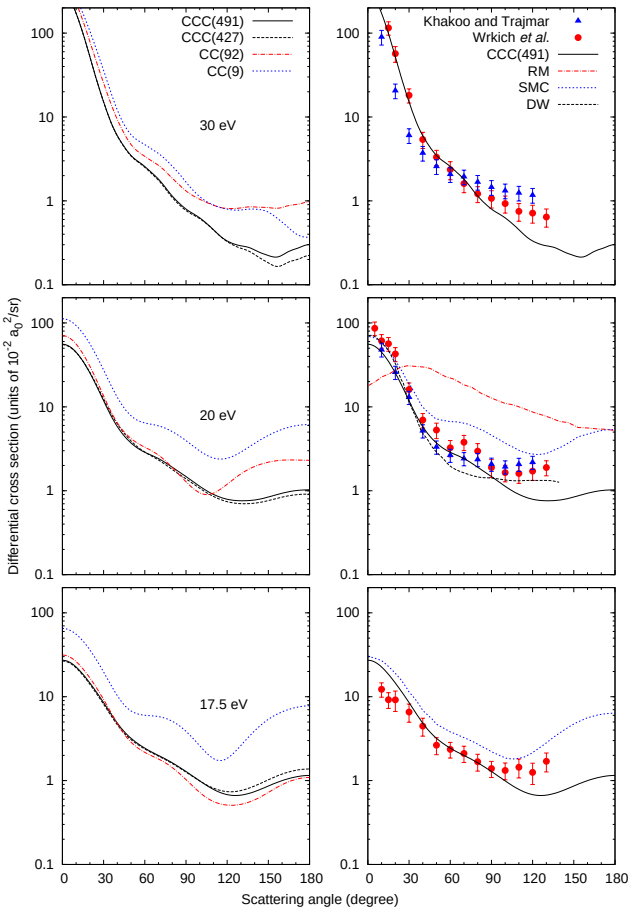

FIG. 21: Electron impact differential excitation cross section of the $C\ ^1\Pi_u$ state of H_2 at 17.5, 20, and 30 eV. The left panel presents convergence studies for the CCC models described in the text and the right panel presents the comparison with the measurements of Wrkich et al. [18] and Khakoo and Trajmar [17], and calculations of Branchett et al. [41] (RM), da Costa et al. [42] (SMC), and Fliflet and McKoy [38] (DW).

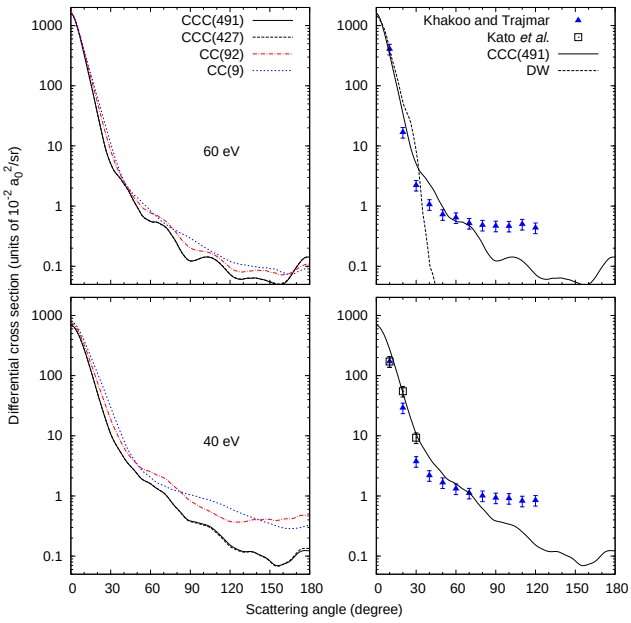

FIG. 22: Same as in Fig. 21 but at 40 and 60 eV. In addition the measurements of Kato et al. [20] are also presented. The DW calculations are due to Mu-Tao et al. [39].

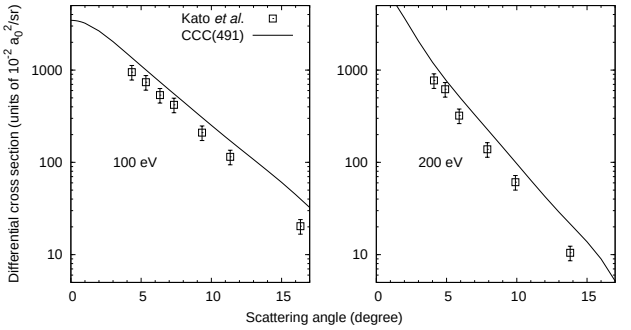

FIG. 23: Same as in Fig. 22 but at 100 and 200 eV.

formulation of the CCC method that makes use of the spheroidal coordinate system. This will allow us to produce AN approximation cross sections for scattering from vibrationally excited states of H_2 and to study the the behavior of the cross sections for energies close to excitation thresholds. The CCC method will also be extended to study collisions with more complicated molecules.

Acknowledgments

This work was supported by the United States Air Force Office of Scientific Research, Los Alamos National Laboratory (LANL) and Curtin University. Zammit would like to specifically acknowledge LANLs ASC PEM Atomic Physics Project for its support. The LANL is operated by Los Alamos National Security, LLC for the National Nuclear Security Administration of the U.S. Department of Energy under Contract No. DE-AC52-06NA25396. Resources were provided by the Pawsey Supercomputing center with funding from the Australian government and the government of Western Australia.

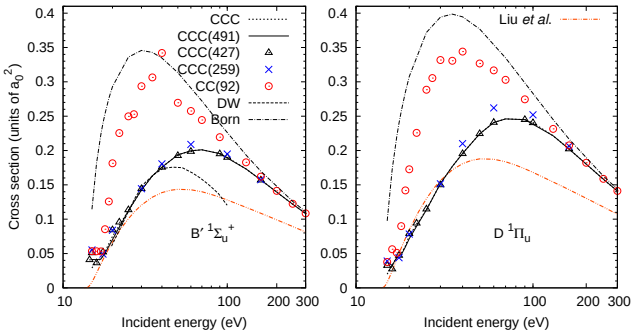

FIG. 24: Electron impact excitation cross sections of the $B'\ ^1\Sigma_u^+$ and $D\ ^1\Pi_u$ states of H_2. Convergence studies are presented for the CCC models described in the text. The exprimental values are due to Liu et al. [26] and DW calculations are due to Mu-Tao et al. [39].

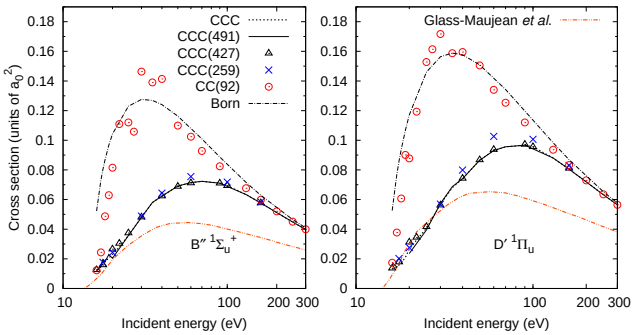

FIG. 25: Electron impact excitation cross sections of the $B''\ ^1\Sigma_u^+$ and $D'\ ^1\Pi_u$ states of H_2. Convergence studies are presented for the CCC models described in the text. The exprimental values are due to Glass-Maujean et al. [27].

[1] J.-S. Yoon, M.-Y. Song, J.-M. Han, S. H. Hwang, W.-S. Chang, B. Lee, and Y. Itikawa, J. Phys. Chem. Ref. Data **37**, 913 (2008).

[2] B. G. Lindsay and M. A. Mangan, *Photon and Electron Interactions with Atoms, Molecules and Ions*, vol. 7 of *Numerical data and functional relationships in science and technology: New series* (Springer, 2003).

[3] M. J. Brunger and S. J. Buckman, Phys. Rep. **357**, 215 (2002).

[4] A. Zecca, G. P. Karwasz, and R. S. Brusa, Riv. Nuovo Cimento **19**, 1 (1996).

[5] J. Ferch, W. Raith, and K. Schroder, J. Phys. B: At. Mol. Opt. Phys. **13**, 1481 (1980).

[6] B. van Wingerden, R. W. Wagenaar, and F. J. de Heer, J. Phys. B: At. Mol. Opt. Phys. **13**, 3481 (1980).

[7] K. R. Hoffman, M. S. Dababneh, Y. F. Hsieh, W. E. Kauppila, V. Pol, J. H. Smart, and T. S. Stein, Phys. Rev. A **25**, 1393 (1982).

[8] A. Deuring, K. Floeder, D. Fromme, W. Raith, A. Schwab, G. Sinapius, P. W. Zitzewitz, and J. Krug, J. Phys. B: At. Mol. Opt. Phys. **16**, 1633 (1983).

[9] R. K. Jones, Phys. Rev. A **31**, 2898 (1985).

[10] K. P. Subramanian and V. Kumar, J. Phys. B: At. Mol. Opt. Phys. **22**, 2387 (1989).

[11] J. C. Nickel, I. Kanik, S. Trajmar, and K. Imre, J. Phys. B: At. Mol. Opt. Phys. **25**, 2427 (1992).

[12] S. Zhou, H. Li, W. E. Kauppila, C. K. Kwan, and T. S. Stein, Phys. Rev. A **55**, 361 (1997).

[13] M. A. Khakoo and J. Segura, J. Phys. B: At. Mol. Opt. Phys. **27**, 2355 (1994).

[14] M. A. Khakoo, S. Trajmar, R. McAdams, and T. W. Shyn, Phys. Rev. A **35**, 2832 (1987).

[15] H. Nishimura and A. Danjo, J. Phys. Soc. Japan **55**, 3031 (1986).

[16] R. I. Hall and L. Andric, J. Phys. B: At. Mol. Opt. Phys. **17**, 3815 (1984).

[17] M. A. Khakoo and S. Trajmar, Phys. Rev. A **34**, 146 (1986).

[18] J. Wrkich, D. Mathews, I. Kanik, S. Trajmar, and M. A. Khakoo, J. Phys. B: At. Mol. Opt. Phys. **35**, 4695 (2002).

[19] S. K. Srivastava and S. Jensen, J. Phys. B: At. Mol. Opt. Phys. **10**, 3341 (1977).

[20] H. Kato, H. Kawahara, M. Hoshino, H. Tanaka, L. Campbell, and M. J. Brunger, Phys. Rev. A **77**, 062708 (2008).

[21] S. Trajmar, D. Register, and A. Chutjian, Phys. Rep. **97**, 219 (1983).

[22] N. J. Mason and W. R. Newell, J. Phys. B: At. Mol. Opt. Phys. **19**, L587 (1986).

[23] X. Liu, D. E. Shemansky, S. M. Ahmed, G. K. James, and J. M. Ajello, J. Geophys. Res. **103**, 26739 (1998).

[24] C. Jonin, X. Liu, J. M. Ajello, G. K. James, and H. Abgrall, ApJS **129**, 247 (2000).

[25] J. M. Ajello and D. E. Shemansky, ApJ **407**, 820 (1993).

[26] X. Liu, P. V. Johnson, C. P. Malone, J. A. Young, D. E. Shemansky, and I. Kanik, J. Phys. B: At. Mol. Opt. Phys. **42**, 185203 (2009).

[27] M. Glass-Maujean, X. Liu, and D. E. Shemansky, ApJS **180**, 38 (2009).

[28] I. Bray and A. T. Stelbovics, Phys. Rev. A **46**, 6995 (1992).

[29] K. Bartschat, E. T. Hudson, M. P. Scott, P. G. Burke, and V. M. Burke, J. Phys. B: At. Mol. Opt. Phys. **29**, 115 (1996).

[30] T. N. Rescigno and B. I. Schneider, J. Phys. B: At. Mol. Opt. Phys. **21**, L691 (1988).

[31] S. D. Parker, C. W. McCurdy, T. N. Rescigno, and B. H. Lengsfield, Phys. Rev. A **43**, 3514 (1991).

[32] M. A. P. Lima, T. L. Gibson, W. M. Huo, and V. McKoy, J. Phys. B: At. Mol. Opt. Phys. **18**, L865 (1985).

[33] T. L. Gibson, M. A. P. Lima, V. McKoy, and W. M. Huo, Phys. Rev. A **35**, 2473 (1987).

[34] M. A. P. Lima, T. L. Gibson, V. McKoy, and W. M. Huo, Phys. Rev. A **38**, 4527 (1988).

[35] B. I. Schneider and L. A. Collins, J. Phys. B: At. Mol. Opt. Phys. **18**, L857 (1985).

[36] A. M. Machado, M. M. Fujimoto, A. M. A. Taveira, L. M. Brescansin, and M.-T. Lee, Phys. Rev. A **63**, 032707 (2001).

[37] T. N. Rescigno, C. W. McCurdy, V. McKoy, and C. F. Bender, Phys. Rev. A **13**, 216 (1976).

[38] A. W. Fliflet and V. McKoy, Phys. Rev. A **21**, 1863 (1980).

[39] L. Mu-Tao, R. R. Lucchese, and V. McKoy, Phys. Rev. A **26**, 3240 (1982).

[40] S. E. Branchett, J. Tennyson, and L. A. Morgan, J. Phys. B: At. Mol. Opt. Phys. **23**, 4625 (1990).

[41] S. E. Branchett, J. Tennyson, and L. A. Morgan, J. Phys. B: At. Mol. Opt. Phys. **24**, 3479 (1991).

[42] R. F. da Costa, F. J. da Paixão, and M. A. P. Lima, J. Phys. B: At. Mol. Opt. Phys. **38**, 4363 (2005).

[43] J. D. Gorfinkiel and J. Tennyson, J. Phys. B: At. Mol. Opt. Phys. **38**, 1607 (2005).

[44] M. S. Pindzola, F. Robicheaux, S. D. Loch, and J. P. Colgan, Phys. Rev. A **73**, 052706 (2006).

[45] R. Utamuratov, A. S. Kadyrov, D. V. Fursa, M. C. Zammit, and I. Bray, Phys. Rev. A **92**, 032707 (2015).

[46] M. C. Zammit, D. V. Fursa, and I. Bray, J. Phys. Conf. Ser. **635**, 012009 (2015).

[47] M. C. Zammit, D. V. Fursa, and I. Bray, Phys. Rev. A **87**, 020701 (2013).

[48] M. C. Zammit, D. V. Fursa, and I. Bray, Phys. Rev. A **90**, 022711 (2014).

[49] M. C. Zammit, D. V. Fursa, and I. Bray, Phys. Rev. A **88**, 062709 (2013).

[50] M. C. Zammit, J. S. Savage, D. V. Fursa, and I. Bray, Phys. Rev. Lett. **116**, 233201 (2016).

[51] D. V. Fursa and I. Bray, Phys. Rev. A **52**, 1279 (1995).

[52] I. Bray, D. V. Fursa, A. S. Kheifets, and A. T. Stelbovics, J. Phys. B: At. Mol. Opt. Phys. **35**, R117 (2002).

[53] D. V. Fursa and I. Bray, Phys. Rev. Lett. **100**, 113201 (2008).

[54] C. J. Bostock, D. V. Fursa, and I. Bray, Phys. Rev. A **82**, 022713 (2010).

[55] N. F. Lane, Rev. Mod. Phys. **52**, 29 (1980).

[56] W. Kolos, K. Szalewicz, and H. J. Monkhorst, J. Chem. Phys. **84**, 3278 (1986).

[57] W. Kolos and L. Wolniewicz, J. Chem. Phys. **43**, 2429 (1965).

[58] W. Kolos and L. Wolniewicz, J. Chem. Phys. **48**, 3672 (1968).

[59] W. Kolos and J. Rychlewski, J. Mol. Spectrosc. **66**, 428 (1977).

[60] G. Staszewska and L. Wolniewicz, Journal of Molecular Spectroscopy **212**, 208 (2002).
[61] J. W. Liu and S. Hagstrom, Phys. Rev. A **48**, 166 (1993).
[62] L. Wolniewicz and G. Staszewska, Journal of Molecular Spectroscopy **220**, 45 (2003).
[63] W. Kolos and J. Rychlewski, J. Mol. Spectr. **143**, 237 (1990), ISSN 0022-2852.
[64] T. E. Sharp, At. Data Nucl. Data Tables **2**, 119 (1971).
[65] L. Wolniewicz and G. Staszewska, Journal of Molecular Spectroscopy **217**, 181 (2003).
[66] G. Staszewska and L. Wolniewicz, Journal of Molecular Spectroscopy **198**, 416 (1999).
[67] W. Kolos and L. Wolniewicz, J. Chem. Phys. **46**, 1426 (1967).
[68] Y. Itikawa, Theor. Chem. Acc. **105**, 123 (2000).
[69] N. Sanna and F. Gianturco, Comp. Phys. Comm. **114**, 142 (1998).
[70] T. N. Rescigno, B. H. Lengsfield, C. W. McCurdy, and S. D. Parker, Phys. Rev. A **45**, 7800 (1992).
[71] R. Zhang, A. Faure, and J. Tennyson, Phys. Scr. **80**, 015301 (2009).
[72] J. Y. Zhang and J. Mitroy, Phys. Rev. A **83**, 022711 (2011).
[73] S. Zhou, H. Li, W. E. Kauppila, C. K. Kwan, and T. S. Stein, Phys. Rev. A **55**, 361 (1997).
[74] D. Rapp and P. Englander-Golden, J. Chem. Phys. **43**, 1464 (1965).
[75] E. Krishnakumar and S. K. Srivastava, J. Phys. B: At. Mol. Opt. Phys. **27**, L251 (1994).
[76] H. C. Straub, P. Renault, B. G. Lindsay, K. A. Smith, and R. F. Stebbings, Phys. Rev. A **54**, 2146 (1996).
[77] J. Tennyson, Comp. Phys. Comm. **100**, 26 (1997).
[78] C. S. Trevisan and J. Tennyson, J. Phys. B: At. Mol. Opt. Phys. **34**, 2935 (2001).
[79] G. Mohlmann and F. de Heer, Chem. Phys. Lett. **43**, 240 (1976), ISSN 0009-2614.
[80] X. Liu, D. E. Shemansky, H. Abgrall, E. Roueff, S. M. Ahmed, and J. M. Ajello, J. Phys. B: At. Mol. Opt. Phys. **36**, 173 (2003).
[81] M. Inokuti, Rev. Mod. Phys. **43**, 297 (1971).
[82] A. Allison and A. Dalgarno, Mol. Phys. **19**, 567 (1970).
[83] G. Arrighini, F. Biondi, and C. Guidotti, Mol. Phys. **41**, 1501 (1980).
[84] I. Borges and C. E. Bielschowsky, Phys. Rev. A **60**, 1226 (1999).
[85] W. Chan, G. Cooper, and C. Brion, Chem. Phys. **168**, 375 (1992).
[86] Z. Zhong, K. Xu, R. Feng, X. Zhang, L. Zhu, and X. Liu, J. Electron. Spectrosc. Relat. Phenom. **94**, 127 (1998).
[87] J. Berkowitz, *Atomic and Molecular Photoabsorption: Absolute Total Cross Sections* (Academic, San Diego, 2002).
[88] TheEditors, Phys. Rev. A **83**, 040001 (2011).
[89] H.-K. Chung, B. J. Braams, K. Bartschat, A. G. Csszr, G. W. F. Drake, T. Kirchner, V. Kokoouline, and J. Tennyson, Journal of Physics D: Applied Physics **49**, 363002 (2016).
[90] L. C. Pitchford, L. L. Alves, K. Bartschat, S. F. Biagi, M.-C. Bordage, I. Bray, C. E. Brion, M. J. Brunger, L. Campbell, A. Chachereau, et al., Plasma Process. Polym. (2016).